MULTISENSOR FUSION FOR PRECISE AGRICULTURE IN PADDY FIELDS

by

Supod Kaewkorn

A Dissertation Submitted in Partial Fulfillment of the Requirements for the Degree of Doctor of Engineering in Mechatronics

Examination Committee:	Dr. Mongkol Ekpanyapong (Chairperson) Prof. Manukid Parnichkun Dr. Attaphongse Taparugssanagorn
External Examiner:	Prof. Joao L. Monteiro Department of Industrial Electronics School of Engineering University of Minho Portugal
Nationality:	Thai
Previous Degree:	Master of Engineering in Electrical Engineering King Mongkut's Institute of Technology Ladkrabang, Thailand
Scholarship Donor:	National Science and Technology Development Agency (NSTDA), Thailand

Asian Institute of Technology
School of Engineering and Technology
Thailand

December 2021

AUTHOR'S DECLARATION

I, Supod Kaewkorn declare that the research work carried out for this dissertation was in accordance with the regulations of the Asian Institute of Technology. The work presented in it are my own and has been generated by me as the result of my own original research, and if external sources were used, such sources have been cited. It is original and has not been submitted to any other institution to obtain another degree or qualification. This is a true copy of the dissertation, including final revisions.

Date: 8 December 2021

Name: Supod Kaewkorn

Signature: 

ACKNOWLEDGMENTS

This work would not have been possible without the financial support of the Ministry of Science and Technology of Thailand. I am especially indebted to Assoc. Prof. Mongkol Ekpanyapong who is the advisor of this research; Prof. Manukid Parnichkun, and Assoc. Prof. Attaphongse Taparugssanagorn who have been supportive of my career goals and who worked actively to provide me with the protected academic time to pursue those goals.

I am grateful to all of those with whom I have had the pleasure to work during this and other related projects. Each of the members of my dissertation committee has provided me extensive personal and professional guidance and taught me a great deal about both scientific research and life in general. I would especially like to thank Dr. Ukrit Thamma, the coworker in my university. As my mentor in my publication, he has taught me more than I could ever give him credit for here. He has shown me, by his example, what a good journal paper should be.

Nobody has been more important to me in the pursuit of this project than the members of my family. I would like to thank my aunt, whose love and guidance are with me in whatever I pursue. She is the ultimate role models. Most importantly, I wish to thank my true friends, who provide unending inspiration.

Finally, I wish to thank Mr. Phakphum Ratchakit, Mr. Montri Sripard, Ms. Tapanee Nachan and Phumpailin team who supported an experimental field and experiments. I would say many thanks for his kind bring the research met the excellent results.

ABSTRACT

Nowadays, the agricultural industry has widely adopted automatic machinery to increase their productivity and reduce production costs. Labor-intensive agricultural tasks are especially targeted to be replaced by an automated robot, such as soil preparation, cultivation, fertilizing, weed control, Insecticide spray, and harvesting. Since these tasks require the robots to follow a predetermined path, one important criteria required from these robots is an accurate and precise localization, which includes XYZ position, heading, and attitude (roll and pitch tilts). This research presents a novel to design, construct a positioning and tilt angle system of agricultural machinery with high precision and low cost using an image-processing triple-laser-guided (TLG) system coupled with an inertial measurement unit (IMU). The TLG system consists of a laser-pointing unit (LPU) at the base station and a laser-target unit (LTU) at the mobile robot. The robot's XYZ position and heading are determined from the positions and the angles relative to the field of both LPU and LTU. The IMU sensor fusion determines the robot's roll and pitch with a complementary filter. The IMU-coupled TLG system was demonstrated on an outdoor, 20 x 21 m flat field at various light intensities, and then tested in an actual paddy field in the same conditions. The paddy field testing indicates that the uneven area of the actual field does not affect the system. The overall lateral and vertical accuracies of the IMU-coupled TLG system are 1.68 cm and 0.59 cm, respectively. The general heading, roll, and pitch accuracies of the IMU-coupled TLG system are 0.90º, 0.78º, and 0.76º, respectively. The lateral and heading accuracies of the IMU-coupled TLG system are comparable to commercially available GNSS-INS systems from NovAtel and Trimble. On the other hand, the total cost of the IMU-coupled TLG system is only a fraction of the total cost of the commercially available localization systems.

Keywords: Laser tracking system, Localization, Inertial Measurement Unit (IMU), Sensor Fusion, Position control.

CONTENTS

LIST OF TABLES

LIST OF FIGURES

LIST OF ABBREVIATIONS

AMU	= Attitude-Measuring Unit
AoA	= Angle of Arrival
A-PPP	= Array-aided Precise point
ASICF	= Adaptive Sparse Interpolation lossless Complementary Filter
CI	= Covariance Intersection
CKF	= Centralized Kalman Filter
CNN	= Convolutional Neural Network
DGPS	= Differential GPS
DML	= Distance-Measuring Laser
DMT	= Distance-Measuring Target
EKF	= Extended Kalman Filter
Faster R-CNN	= Faster Regional-Convolutional Neural Network
FMCW	= Frequency Modulation Continuous Wave
FOV	= Field Of View
FVCU	= Fanning-Vertical Control Unit
GL/YRS	= G sensors/Yaw Rate Sensor
GLTN	= Goddard Laser Tracking Network
GNSS	= Global Navigation Satellite System
GPS	= Global Positioning System
HCU	= Heading Control Unit
HML	= Heading-Measuring Laser
HMT	= Heading-Measuring Target
ICP	= Iterative Closest Point
IMU	= Inertial Measurement Unit
INS	= Inertial Navigation Systems
IoT	= Internet of Things
IPSs	= Indoor Positioning Systems
IR	= Infrared
ISN	= Intelligent Sensor Nodes
LiDAR	= Light laser Detection And Ranging
LMB	= Labeled Multi-Bernoulli

LOAM = LiDAR Odometry And Mapping
LoRa = Long Range
LPU = Laser-Pointing Unit
LRF = Laser Range Finder
LTS = Laser Tracking System
LTU = Laser-Target Unit
ML = Maximum Likelihood estimators
MEMS = Micro-Electro-Mechanical Systems
METT = Multi-Extended Target Tracking
MTDTS = Multi-Target Detection and Tracking System
NMPC = Nonlinear Model Predictive Control
PA = Precision Agriculture
PFC = Path-Following Controller
PML = Position-Measuring Laser
PMT = Position-Measuring Target
PSD = Position-Sensitive Detector
RFID = Radio-Frequency Identification
RFS = Random Finite Set
RMSE = Root Mean Square Error
RSS = Received Signal Strength
RSSI = Received Signal Strength Indicator
RTK = Real Time Kinematic
RWHT = Range Weighted Hough Transform
SALA = Smartphone Assisted Localization Algorithm
SD, STD = Standard Deviation
SDF = Sensor Data Fusion
SLAM = Simultaneous Localization And Mapping
TLG = Triple-Laser-Guided
TOA = Time Of Arrival
UGV = Unmanned Ground Vehicle
UTV = Unmanned Terrestrial Vehicles
UWB = Ultra Wide Band
VI-SLAM = Visual-Inertial SLAM

VPE = Vehicle's Pose Estimator

WSN = Wireless Sensor Network

WSS = Wheel Speed Sensor

CHAPTER 1
INTRODUCTION

1.1 Background of the Study

In recent years, automatic guidance machinery for farming has been widely researched and implemented in the agricultural industry to increase productivity and reduce costs. Specifically, automatic guided robots support many agricultural tasks, i.e., seeding, weed controlling, soil tilling, fertilizing, watering, and harvesting. Most automatic farming uses Global positioning system (GPS) and machine vision mainly. The accuracy was 25 mm and 60 mm, respectively (Reid et al., 2000). Using GPS for outdoor location and RF-base trilateration for indoor was proposed by Borenstein et al. (1997). Many sensors and methodologies were studied to compare and find the best solution suitable for applications (Hague et al., 2000). The position estimator method, named maximum likelihood (ML), is applied to get the highest position accuracy (Zekavat and Buehrer, 2011). The technology expanded fastly; in a short year, navigation systems developed for US agriculture were born; for example, a transplanting robot can travel within an error range of ±100 mm from the predetermined path. RTK-GPS is popular equipment that offers position accuracy down to 20 mm (Zhang and Pierce, 2013), but it has many errors in heading measurement.

An inertial measurement unit (IMU) is an electronic device that also measures acceleration, angular velocity, and magnetic field. Both acceleration and angular velocity output of IMU can calculate their tilts using the sensors fusion technique (Min and Jeung, 2015; Zhe et al., 2020). In order to get good accuracy in tilts measurement, complementary filter and Kalman filter are applied in many applicable cases (Pititeeraphab et al., 2016). Gui et al. (2015) and Ngo et al. (2017) reported that the comparison results of the complementary filter could be more stable and accurate than the Kalman filter. Filtering and adding more IMU are also used to improve tilt measurement accuracy down to 0.004 deg (Weng et al., 2017).

In order to save sensing equipment costs and obtain more accuracy, multi-sensor fusion is a regularity to reduce the cost and improve the system performance. Zhu et al. (2011); Emter and Ulrich (2012); LeVoir et al., (2020) presented camera fuse with

LiDAR. The results look pretty good; position cross-track SD reaches 13.7 mm, and angle cross-track SD is about 0.93 deg during the late-growth season. Range measurement by the time of arrival (TOA) gives high accuracy (Zekavat and Buehrer, 2011); the distance error is less than 10 mm and low cost. The sensor made by TOA can use with each other to identify the position. More sensor fusion techniques with GPS (Gomez-Gil et al., 2011; Singh et al., 2019), differential GPS (DGPS) (Emter et al., 2010), global navigation satellite system (GNSS) (Sippel et al., 2008; Guo et al., 2018), real time kinematic GPS (RTK-GPS) (Lenain et al., 2006; Han et al., 2015), RTK-DGPS (Gan-Mor et al., 2007), RTK-GNSS (Jilek, 2015; Tatarnikov et al., 2017; Pini et al., 2020), camera (Betke and Gurvits, 1997; Shim and Cho, 2015), encoder (Shalal et al., 2015a; Nemec et al., 2019), IMU (Shalal et al., 2015b; Le et al., 2019), Magnetic sensors (Sheinker et al., 2013; Nilwong et al., 2019), ultra wide band (UWB) (Shi et al., 2020), radar (Guan et al., 2018), ultrasonic (Hoppenot and Colle, 1997), radio frequency (RF) (Hsu et al., 2007), laser beacons based (Moreira et al., 2020), infrared (IR) landmark (Her et al., 2012), optical sensor (Corbellini et al., 2006; Souvestre et al., 2009), Position-Sensitive Detector (PSD) (De-La-Llana-calvo et al., 2020), laser range finder (LRF) (Larsson et al., 1996; Bento et al., 2005; Libby and Kantor, 2011; Canedo-Rodríguez et al., 2016) describe in chapter 2 literature reviews.

Mainly, farmers employ RTK GNSS coupled with inertial navigation systems (INS) extensively due to its relatively higher accuracy and precision than other sensing techniques. In the RTK GNSS-INS system, the robot's position is determined based on the trilateration of the Universal Transverse Mercator obtained through a constellation of satellites. In contrast, the robot's heading and attitude are obtained by real-time measurements of angular velocity, linear acceleration, and the earth's magnetic field via the INS.

Nonetheless, there are a few drawbacks to the agricultural practicality of the RTK GNSS-INS system:

1. The RTK GNSS-INS system's accuracy and precision depend on the transmissivity of satellites' signals. The decrease in the satellite transmissivity due to signal blockage from neighboring buildings or trees and cloudy weather

can deteriorate the RTK GNSS-INS system's positioning accuracy and precision.

2. The heading determination in the RTK GNSS-INS system partly relies on the sensor fusion between the earth's magnetic field measurement from magnetometers and the angular velocity measurement from gyroscopes with tilt compensation accelerometers in the INS unit. Due to geographical variation in the earth's magnetic field, the RTK GNSS-INS system requires a time-consuming calibration when the operating field has been moved.
3. The earth's magnetic field measurement can easily be interfered with by the surrounding environment, such as motor, metallic structures, and electronic equipment; therefore, the INS's heading measurement can be inconsistent and unreliable.
4. The RTK GNSS-INS system is currently costly and not affordable to small-scale farming operations.

In order to compensate for the drawbacks of an expensive RTK GNSS-INS system, this research presents a low-cost, inertial measurement unit (IMU)-coupled triple-laser-guided (TLG) system with superior localization accuracy and precision at a substantially lower cost.

1.2 Statement of the Problem

This research considers a solution to locate a robot position in the paddy field, which solves problems in the list below:

- Low-accuracy and precision that is not enough for a robot in a paddy field
- The expensive of the RTK-INS navigation system in markets
- Signals blocked in low RF signals (Both satellite and RF communication signal) areas, such as urban areas with buildings, dense forests, and cloudy days.
- Tilts compensation for end-effector
- Robust against electromagnetic field
- Easy for carry-on and installation.

1.3 Research Questions

The list below is shown the research questions. The answer will be evident to decide an appropriate localization system for autonomous machinery systems in outdoor and indoor environments.

- Can the system work under sunlight directly and indirectly?
- How much light intensity that the system can work?
- What is the limitation of measurement?
- What is the accuracy and precision of position and attitude?
- How to apply with an autonomous farming robot?
- How much does it cost?
- What is the strategy to implement the localization system?
- How to track the target in the paddy field?
- What is the best sensor for sensing laser points?
- How to test and get the performance, accuracy, and precision of the system?
- How is the system robust against electromagnetic field interferences and environmental influences?

1.4 Objectives of the Study

The main objective of this study in the list below answers the research question above. The objective of the study is in the following topic:

- To develop low-cost multisensor fusion with the 5 cm. precision
- To demonstrate the actual deployment both in actual flat field and in paddy field
- To compare with commercial outdoor localization systems based on RTK

1.5 Scope and Limitations

The scope and limitations of this research are listed as follows:

- The robot speed is equal to or less than 2 m/S
- No intensity sunlight at laser target sensor directly
- The working area is 20 x 20 m
- Ground slope less than 45 degree
- No laser blocked between laser base and laser target scene
- Low moisture area.

1.6 Contributions and Publications

There is a contribution in IEEE access publication which includes all concepts and designs to get indoor and outdoor robot position and attitude in a flat field. The publication is “S. Kaewkorn, M. Ekpanyapong and U. Thamma, "High-Accuracy Position-Aware Robot for Agricultural Automation Using Low-Cost IMU-Coupled Triple-Laser-Guided (TLG) System," in IEEE Access, vol. 9, pp. 54325-54337, 2021, doi: 10.1109/ACCESS.2021.3071554.”. Readers can access for free via “https://ieeexplore.ieee.org/xpl/RecentIssue.jsp?punumber=6287639”.

1.7 Organization of the Study

This dissertation is organized into five main parts. The chapters are divided into subtopics: Chapter 1 introduces the background of study in high-accuracy robot position and tilts for agriculture and their system with literature reviews. Both indoor and outdoor technics are discussed to summarize the advantage and disadvantages in various views. The sub-chapter objectives of the study and scope show the aims of this research in bullet points. Moreover, an IEEE Access publication with an impact factor of 3.367 is presented. Chapter 2 summarizes literature reviews in tables and discussions by listed groups of sensor types and reported their brief details, accuracy in position errors, and tilt errors. Chapter 3 describes the system equipment of the laser base station and the mobile unit in the first and second sub-chapter, respectively. In order to succeed in the measurement system, all parameters from sensors, data communication, control strategies, and determination of robot’s position and pose are shown in this chapter. The experimental results are then in chapter 4. Conclusions, discussions, and recommendations for future work contain in chapter 5.

CHAPTER 2
LITERATURE REVIEWS

In this chapter, localization systems for agricultural applications for both indoor and outdoor environments including historical products and research studies are summarized in terms of accuracy, precision, worthiness, technology, difficulty, and efficiency. The total of 72 published research and books is reviewed, summarized, and rewritten in 10 tables with descriptions—the information guide to decide a new localization system that is better than the old one.

To begin the study of localization for a robot in a paddy field, pieces of knowledge about agriculture machinery are essential.

2.1 Localization Methodology for Agriculture

The literature review begins with searching manuscripts and books from the websites. The best research searching is "Google Scholar," which can feed a lot of research knowledge about robot localization in the paddy field with their details. Mendeley, a citation managing tool, is used to help collect bibliographical information and correctly generate a reference list. The 23 historical types of research from 1997 to 2020 in Table 2.1 are reviewed to study automatic guidance robots.

The studying and development of robot navigation systems started before 1990. The purpose is to make a farming machine work in fields automatically (Borenstein et al., 1997). There are two main types of position sensors, which are absolute measurement sensors and relative measurement sensors. The absolute measurement can determine the robot's position in reference to the geographical coordinate, so the information from the sensor identifies the place in latitude and longitude. In comparison, the relative measurement determines the robot's coordinate relative to a local reference. For example, the navigation solution for the outdoor environment is GPS (absolute), and the answer for the indoor climate is RF-based trilateration (relative) via triangulation (Borenstein et al., 1997).

GPS has become a widely adopted sensor to measure a point on ground location because of easy use, low cost, and lightweight, but it has low accuracy and low precision (Position error up to 25 m). Therefore, GPS with ground base compensation

(RTK-GPS) is developed to further minimize the positioning error; the total displacement SD is 13.4 mm designed with RTK-GPS + IMU + Odometer for a John Deer tractor model 6430 (Perez-Ruiz et al., 2012).

Although, RTK-GPS has high accuracy enough for agriculture, there are some drawbacks, for examples, low satellite signals and tall building signal block and reflection those lead to low position accuracy.

Satellite signal blocked, and low heading accuracy of RTK can be improved by sensor fusion methodology. Local relative position sensors such as cameras (Shalal et al., 2015a) and laser scanners (Backman et al., 2012) are used to identify the position in RTK blocked time.

IMU is presented to improve heading accuracy because IMU can measure tilt quickly and accurately. The tilts accuracy measure by IMU sensor fusion is 0.2˚ (Zhang and Pierce, 2013).

Table 2.1

Review on Localization Methodology for Agriculture

Author	Sensors	Strategies	Experimental	Accuracy (mm)
(Borenstein et al., 1997)	Review	A review on mobile robot positioning & sensors and techniques in seven categories for positioning systems: 1. Odometry; 2. Inertial Navigation; 3. Magnetic Compasses; 4. Active Beacons; 5. Global Positioning Systems; 6. Landmark Navigation; and 7. Model Matching	Review	The navigation solution: - Outdoor is GPS - Indoor is RF-base trilateration using triangulation. The results are in appendix A
(Reid et al., 2000)	Review	Review navigation system sensors such as: Mechanical feelers, Machine vision, Global position systems, Geomagnetic direction sensor Review Navigation planner such as: Dead reckoning, Kinematic model, Sensor fusion, Autonomous functions	Review	Most of the navigation system developed for US agriculture is machine vision, and GPS techniques are: Machine vision gives 60 mm accuracy at 4.9 km/h, GPS has line tracking accuracy of 25 mm and 1 deg accuracy in the heading.
(Hague et al., 2000)	Review in Odometer, IMU, Laser range finder, Radar, Sonar, Camera	To examine ground-based sensing systems for autonomous agricultural vehicles in various sensor categories	Review	The summary of position offset error of sensors in Fig. 5 shows the best accuracy is sensors fusion with Kalman filter, which is within 50 mm
(Corbellini et al., 2006)	Laser + Optical sensor	Detecting laser light rotating with an optical sensor to get the tractor position	A tractor with the position in fields up to 0.5 km	Different distance SD: - Raw data 1500 mm at a distance of 250 m - Filtered data 700 mm at a distance of 250 m
(Gan-Mor et al., 2007)	RTK-DGPS	Improve the accuracy by using a three-point hitch implement mounted on RTK-DGPS for a tractor	The testing system and a tractor	RMSE of the lateral deviations: 69.1 mm and 74.1 mm for speed 4.0 and 7.2 km/h, respectively
(Rovira-Más et al., 2008)	RTK-GPS + Stereo camera + IMU	A 3D terrain map by a stereo camera and localization aid sensors (RTK-GPS, IMU)	A utility vehicle (John Deere, Moline, IL)	The system can generate 3D field maps for precision agriculture, as shown in Fig. 9, 11, and 13

Author	Sensors	Strategies	Experimental	Accuracy (mm)
(Nagasaka et al., 2009)	GPS + IMU + Encoder	Development of an automated rice transplanter guided by a global positioning system, an inertial measurement unit, and rotary encoder	A rice transplanter in a paddy field	RMS lateral deviation was observed to be < 40 mm, RMS heading Error was < 3.6 deg
(Sun et al., 2010)	RTK-GPS + IMU + Encoder	Design a positive-placement vegetable crop transplanter retrofitted with an RTK GPS receiver, plant, inclination, and odometry sensors	Self-developed Row-crop transplanter	The mean of position Error is 20 mm
(Gomez-Gil et al., 2011)	GPS	GPS data and tractor kinematic control laws fusion by placing the GPS receiver ahead of the tractor and applying kinematic laws of tractor movement	Simulation and tested with a tractor on a field	RMS Error: 48 mm at 5 m of forwarding GPS guidance position
(Libby and Kantor, 2011)	Laser range finder + Encoder	Uses wheel odometry and laser rangefinder with an extended Kalman filter (EKF) algorithm for localizing a mobile robot in an orchard environment	Self-testing system in an orchard	The mean crosstrack Error is 140 mm The mean downtrack Error is 160 mm
(Zekavat and Buehrer, 2011)	Book	Handbook of position location	The book describes all about position and location	Features: Table 1.1. Comparison of basic methods, Table 1.2. Comparison of positioning systems (Part 1), Table 2.2. Comparison of different measurement models, Table 2.3. Comparison of different position estimators The viewpoint: TOA gives high accuracy
(Backman et al., 2012)	GPS + Laser scanner + IMU	Navigation system for agricultural machines using Nonlinear Model Predictive Control (NMPC) with GPS, 2D laser scanner, and IMU fused with extended Kalman filter (EKF)	Tractor and trailer system	The accuracy requirement was at most 100 mm; lateral Error at a speed of 12 km/h
(Perez-Ruiz et al., 2012)	RTK-GPS + IMU + Odometer	Geospatial mapping of transplanted tomato plant using RTK-GPS on a tractor and IMU and absolute shaft encoder on a transplanter	A tractor (John Deere model 6430 and transplanter (model 1600)	Easting displacement SD is 19.2 mm, Northing displacement SD is 23.0 mm, Total SD is 13.4 mm
(Xue et al., 2012)	RTK-GNSS + 2D-LiDAR	Using a camera with pitch and yaw motion control to navigate between rows in cornfields	Self-developed robot platform in a cornfield	The maximum guidance Error is 15.8 mm

Author	Sensors	Strategies	Experimental	Accuracy (mm)
(English et al., 2013)	GPS + INS + Camera	Positioning system using pose estimation by fusing data from a low-cost global positioning sensor, low-cost inertial sensors, and a new technique for vision-based row tracking algorithm to improve the performance of the positioning system	A testing robotic platform designed for spraying weeds	RMS Error: - Skytraq (RTK GPS)+row tracking is 80 mm - uBlox (GPS) + row tracking is 520 mm
(Zhang and Pierce, 2013)	book	Agricultural automation fundamentals and practices	Book	The famous sensor for agriculture robots is RTK-GPS. The RTK-GPS has an accuracy of ±2 cm, whereas the IMU composed of fiber optics gyroscope has an accuracy of 0.2° (P16)
(Han et al., 2015)	RTK-GPS+IMU	Auto-guidance tillage tractor for a paddy field in Korea using look-ahead distance method for controlling the tractor with RTK-GPS and GNSS-INS sensor fusion	Tillage tractor with sensors and actuators	RMS lateral Errors: - Straight paths is ranging from 38 mm to 128 mm, - Moisture (content > 30%) is 1000 mm
(Shalal et al., 2015a)	Camera + Laser scanner + IMU + Odometers	Using tree trunk orchards detection algorithm with a camera and laser scanner data fusion, tested in sunny and cloudy days	CoroWare Explorer platform with on-board sensors	Tree trunks and non-tree objects with the detection accuracy of 96.64%
(Guo et al., 2018)	GPS, GNSS, RTK	Examination of the feasibility of multi-GNSS precise point positioning (PPP) in precision agriculture (PA) compared with GPS only and RTK	Self-testing system	Multi-GNSS improved the accuracy of base-line length from 126.0 mm to 35.0 mm and the repeatability from 110.0 mm to 49.0 mm, in addition to the BeiDou, Galileo, and GLONASS positioning accuracy of 20 mm
(YIN et al., 2018)	RTK-GNSS + IMU	Implementation of rice transplanter automatic guidance with RTK-GNSS and IMU fusion	The automatically guided rice transplanter	Position Error < 100 mm
(Pini et al., 2020)	RTK-GNSS	RTK-GNSS experimental to get methodologies for use in precision agriculture	Real field test in different environments	Position Error < 25 mm
(Li et al., 2020)	Dual antenna RTK-GNSS	Use dual antenna GNSS for land leveling equipment	A tractor with land leveling equipment	SD of land leveler: Before leveling is 74.4 mm, After leveling is 12.6 mm

Author	Sensors	Strategies	Experimental	Accuracy (mm)
(LeVoir et al., 2020)	Camera + LiDAR	Develop a high-accuracy adaptive low-cost location by using the camera, and a LiDAR for precision agriculture (PA) by machine-learning	Self-developed the "bikebot"	Cross-track SD: - During growth season is 25.1 mm, - During the late growth season is 13.7 mm

2.2 Using Sensors for Indoor and Outdoor Localization

To design the localization measurement system, the location application is divided into two scenarios, indoor and outdoor environments. The system designers must understand sensors' features and properties to pick suitable sensors for their application. Sensor review for indoor and outdoor localization system is summarized here in this section where the sensors were divided into two main categories: absolute position sensor in table 2.2-2.3 and relative position sensor with tilts sensor in Table 2.4.

2.2.1 Absolute Position based on Satellite Signals and Ground Base Station

Table 2.2 lists localization techniques using absolute position based on satellite signals. The GPS and GNSS are used as the primary sensor to obtain robot positions in the outdoor environment. The difference between GPS and GNSS is GPS receives signals from only one group of satellites named GPS, while GNSS receives the signals from multi-satellite such as the United States' Global Positioning System (GPS), Russia's Global Navigation Satellite System (GLONASS), China's BeiDou Navigation Satellite System (BDS), and the European Union's Galileo.

There are many types of research in GPS and GNSS systems fusion with other sensors to increase precision and accuracy, as shown in Table 2.2. One interesting case is Mizushima et al. (2011) study using three vibratory gyroscopes and two inclinometers sensor fusion for a roll, pitch, and heading measurements with improved GPS position accuracy. The outdoor positioning accuracy reduced from 259 mm to 30 cm on a sloping ground and 84 mm to 37 mm a rough terrain. The maximum orientation error (RMS) of roll, pitch, and yaw are 0.43˚, 0.61˚, and 0.64˚, respectively.

Table 2.2

Review on Localization by using Absolute Position based on Satellite Signals

Author	Sensors	Strategies	Application	Experimental	Position Accuracy (mm)	Orientation Accuracy (deg)
(Gao et al., 2007)	GPS + IMU + WSS + GL/YRS	Develop a GPS, low-cost IMU, and onboard vehicle sensors integrated land vehicle positioning system using a centralized Kalman filter	Outdoor	The system on a car	Horizontal position difference RMS is 380 mm	N/A
(Sippel et al., 2008)	GNSS + Laser tracking	Design of a laser tracking system for GNSS augmenting	Outdoor	Real railway tracking model	Maximum absolute position Error is 65 mm	N/A
(Nagasaka et al., 2009)	GPS + IMU + Encoder	Development of an automated rice transplanter guided by a GPS, IMU, and rotary encoder	Outdoor	A rice transplanter in a paddy field	Lateral deviation RMS was observed to be < 40 mm	Heading angle RMS Error was < 3.6 deg
(Lee et al., 2009)	GPS + Camera + Odometer	Development of robot localization using camera fuse odometer with particle filter and GPS with Kalman filter	Outdoor	A mobile robot	Average position Error: X is 780 mm and Y is 430 mm	N/A
(Weinstein and Moore, 2010)	GPS + IMU, Potentiometer + Encoder	A localization scheme for Ackerman steering vehicles using a low-cost GPS and inclinometer fusion by complementary filter and Kalman filter to estimate the vehicle's pose. A string potentiometer and an encoder to determine the vehicle steering angle and the speed	Outdoor	The electric mini-Baja vehicle	Results in the position plot seem reasonable, as shown in Fig. 8	N/A
(Emter et al., 2010)	DGPS + IMU + Odometer+ Compass + LiDAR + ToF camera	Multi-sensor fusion for a total 6 DoF estimation of position and attitude in outdoor environments using a new Kalman filter	Outdoor	A mobile robot	The plotting results in maps look smoother with filtered and odometry has error when moving for a long time as shown in Fig. 3-6	N/A

Author	Sensors	Strategies	Application	Experimental	Position Accuracy (mm)	Orientation Accuracy (deg)
(Gomez-Gil et al., 2011)	GPS	GPS data and tractor kinematic control laws fusion by placing the GPS receiver ahead of the tractor and on applying kinematic laws of tractor movement	Outdoor	Simulation and testing with a tractor	Position Error RMS is 48 mm at 5 m of forwarding GPS guidance position	N/A
(Mizushima et al., 2011)	GPS + Gyroscope + Inclinometer	Three vibratory gyroscopes and two inclinometers sensor fusion to get a roll, pitch, and heading with improved GPS position accuracy	Outdoor	A prototype of the attitude sensor	Improved the positioning accuracy from 259 mm to 30 mm in the sloping ground from 84 mm to 37 mm in the bumpy road	Max Error RMS: - roll 0.43 deg, - pitch 0.61 deg, - heading 0.64 deg
(Li et al., 2012)	GPS + Laser range finder + Encoder	Localization algorithm for the outdoor navigation system, using cubature Kalman filter based on standard dead reckoning sensors and laser range and bearing information	Outdoor	Simulation	Cubature Kalman filter performs much better than using the extended Kalman filter by fixed 10 mm accuracy for simulation	N/A
(Backman et al., 2012)	GPS + Laser scanner + IMU	Navigation system for agricultural machines using nonlinear model predictive control (NMPC) with GPS, 2D laser scanner, and IMU fused by extended Kalman filter (EKF)	Outdoor	Tractor and trailer system	Accuracy requirement was at most 100 mm lateral Error at a speed of 12 km/h	N/A
(English et al., 2013)	GPS + INS + Camera	Positioning system using pose estimation by fusing data from a low-cost GPS, low-cost IMU, and a new technique for vision-based row tracking algorithm to improve the performance of the positioning system	Outdoor across a 6 hectare field.	Robotic platform designed for spraying weeds	Error RMS: - Skytraq (RTK GPS) + row tracking is 80 mm, - uBlox (GPS) + row tracking is 520 mm	N/A
(Wei et al., 2013)	GPS + Camera + Laser range finder	A stereoscopic system, a laser range finder (LRF), and a global localization sensor GPS, fused with an unscented information filter	Outdoor	A 4 wheels vehicle	Position error SD: Minimum Error of Unscented IF (UIF) fusion (with rejection) is 1080 mm	N/A

Author	Sensors	Strategies	Application	Experimental	Position Accuracy (mm)	Orientation Accuracy (deg)
(Singh et al., 2019)	GPS	A design of connecting a robot with GPS locating to a Wi-Fi modem and a GPRS modem for sending robot position and heading to IoT server	outdoor	Mobile robot	The robot location accuracy result is relatively low, as shown in the section result and discussion picture, which shows a path plot on Google Earth	N/A

Nowadays, the positioning triangulation from the GPS/GNSS satellites has been improved by adding a base station compensator, namely real-time kinematic (RTK), to reach high accuracy down to a bit of a millimeter. Since the RTK base station is stationary, it improves the prevision and accuracy of the robot localization using transmitted compensation information set to the rover receivers via a radio frequency signal.

The three types of RTK system is reviewed in Table 2.3 with positioning accuracy. The RTK-GPS by Lenain et al. (2006) integrated with control raw had a tracking error in range ±150 mm, while RTK-GNSS (Jilek, 2015) has reported a position error under 10 mm. The accuracy of RTK-GNSS can be further improved by using dual-frequency antennas named "Backfire helix" with positioning error of 1.5 mm in vertical direction and below 1 mm in the horizontal plane (Tatarnikov et al., 2017). RTK-DGPS is a way to increase position accuracy; Gan-Mor et al. (2007) reported that RTK-DPGS gives RMSE of the lateral deviations 69.1 mm and 74.1 mm for speed 4.0 and 7.2 km/h, respectively.

Table 2.3

Review on Localization by using Satellite Signals with Ground Base Compensation

Author	Sensors	Strategies	Application	Experimental	Position Accuracy (mm)	Orientation Accuracy (deg)
(Lenain et al., 2006)	RTK-GPS	Use control raw with RTK-GPS to get high-accuracy path tracking for farm vehicles and anti-sliding	Outdoor	Vehicles used in actual experiments	Tracking Error remains in the target range ±150 mm	N/A
(Gan-Mor et al., 2007)	RTK-DGPS	Improve the accuracy by using a three-point hitch implement mounted on RTK-DGPS for a tractor	Outdoor on paved and rough surfaces	The testing system and a tractor	RMSE of the lateral deviations: 69.1 mm and 74.1 mm for speed 4.0 and 7.2 km/h, respectively	N/A
(Jilek, 2015)	RTK-GNSS	Field measurements in outdoor environments using RTK-GNSS	Outdoor	Orpheus-X3 mobile robot	Predicted Errors are under 10 mm	N/A
(Tatarnikov et al., 2017)	RTK-GNSS	Using dual frequency Backfire helix antennas for RTK to get high precision positioning	Outdoor	Testing system	Positioning Error is estimated as 1.5 mm in vertical and below 1 mm in the horizontal plane in the RMS sense	N/A

To design a high-performance locating system, the modified RTK and sensor fusion are applied, as presented in Table 2.4. By using Two RTK (De-La-Llana-calvo et al., 2020; Valente et al., 2020), the average positioning error were improved to be less than 30 mm (Aghili and Salerno, 2009). In addition, multi-antenna RTK is a strategy to achieve a higher accuracy (LI and Teunissen, 2012). RTK sensor fusion is also developed to improve position and orientation accuracy (Fang et al., 2009; (Kato and Morioka, 2019; He et al., 2020).

The information in table 2.4 is a review of localization by using modified RTK in several techniques and their results from 2009 to 2021. Using RTK-GNSS + IMU + UWB is shown to be one of the best indoor/outdoor options for positioning and orientation system. The position error is 15 mm, and the heading error is 0.05˚ at a baseline of 10 m.

Table 2.4

Review on Localization by using Modified RTK by Specific Techniques

Author	Sensors	Strategies	Application	Experimental	Position Accuracy (mm)	Orientation Accuracy (deg)
(Aghili and Salerno, 2009)	two RTK-GPS + IMU	Mobile robot localization using Kalman filter with 2 RTK(GPS) + IMU fusion for driftless 3-D attitude determination and robot position estimate	Outdoor	Canadian Space Agency (CSA)	- Attitude estimation exhibits have no drifting, - Average position Error is 30 mm, - Max Error is 120 mm	N/A
(Fang et al., 2009)	RTK + Camera + Odometers	Ground-texture-based localization by mounted a camera at the bottom of a vehicle, odometry, and RTK to create the mapping	Outdoor	A vehicle	Position Error: - X is 62.8 mm, - Y is 63.9 mm	Heading Error is 0.78 deg
(LI and Teunissen, 2012)	Multiple antennas RTK	Improving long-baseline RTK positioning (80 km) with multiple antennas dual-frequency GPS data by using Array-aided precise point positioning (A-PPP)	Outdoor	Self-testing system	STD of ARTK: - North is 54 mm, - East is 59 mm, - Up is 38.9 mm	N/A
(Kato and Morioka, 2019)	RTK-GNSS + 2D-LiDAR	Use deep reinforcement learning and localization using RTK-GNSS; the robot can take adequate action from obstacle positions obtained from 2D-LiDAR	Outdoor	Self-developed autonomous mobile robot	Accuracy of several centimeters within 10 km in general urban environments	N/A
(De-La-Llana-calvo et al., 2020)	Two RTK-GNSS	Evaluate two low-cost RTK-GNSSs in terms of positioning accuracy and precision	Outdoor	Self-developed mobile robot	Root Mean Square Error (RMSE) < 50 mm	N/A
(Valente et al., 2020)	Two RTK-GNSS	Improve two RTK-GNSS by mounted on a fixed, known distance between the GNSS antennas on the robot (472 mm)	Outdoor	RTK-GNSS and a tester robot	Root Mean Square Error (RMSE) < 50 mm	N/A

Author	Sensors	Strategies	Application	Experimental	Position Accuracy (mm)	Orientation Accuracy (deg)
(He et al., 2020)	RTK-GNSS + LiDAR	An integrated localization and mapping (SLAM) by dual-antenna GNSS positioning and LiDAR-SLAM	Large-scale outdoor environments	Unmanned ground vehicle (UGV)	Mean Error: - X 260 mm, - Y 290 mm, - Z 370 mm	Mean Error: - Yaw is 0.73 deg, - Pitch is 1.289 deg
(Zhang et al., 2020)	RTK-GNSS + IMU + UWB	Use IMU, UWB, and dual-antenna RTK-GNSS fusion by Kalman filter for Indoor/Outdoor positioning and orientation	Indoor / outdoor with positioning and orientation system	Real testing system	Position Error is 15 mm (Single baseline RTK)	- Heading Error is 0.09 deg at baseline 2 m - Heading Error is 0.05 deg at baseline 10 m
(Dai et al., 2020)	RTK-GNSS + IMU + Laser range finder	Intertarget Occlusion Handling in Multiextended Target Tracking (METT) Based on Labeled Multi-Ber noulli (LMB) Filter	Outdoor	Ego vehicle equipped with sensors	The system can estimate tracks (no satellite signal); the results are shown in Fig. 11 and Fig. 13	N/A
(Niu et al., 2020)	RTK + Camera	Combination of RTK and VI-SLAM based on smartphones	Indoor / Outdoor	Urban areas	RMS Error : GNSS-hostile area: - RTK 5441.2 mm, - VI-SLAM 5402.1 mm GNSS-allowed area: - RTK 1376.1 mm, - VI-SLAM 5391.9 mm	N/A
(Mayer et al., 2021)	RTK-GNSS + LoRa	An energy-efficient RTK-based system using low-power long-range communication (LoRa) to communicate with RTK base	Outdoor	Real field testing	Base- Rover distance in kilometers of distance: - Overall Position Error 200 mm, - Peak Error < 100 mm	N/A

2.2.2 Relative Position and Tilts

A local positioning system is a technique to complete a localization system. A camera, a laser scanner, an IMU, and an odometer are necessary sensors to develop such system. Table 2.5 is the summary of a review of the necessary positioning and orientation sensors for robot's relative location and its pose. Camera + LiDAR gives position error in range ± 150 mm, while Camera + Laser scanner + IMU + Odometers can get 103 mm of the average position error RMS. Although image processing using neuron networks is developed, the accuracy is still low (Nilwong et al., 2019).

Table 2.5

Review on Localization by using Camera with Sensors Fusion

Author	Sensors	Strategies	Application	Experimental	Position Accuracy (mm)	Orientation Accuracy (deg)
(Betke and Gurvits, 1997)	camera	An algorithm to estimate robot localization using landmarks with well-known triangulation techniques. sensors can be cameras or others	Simulation	Simulation with/without the outlier landmarks	Length of the vector Error: - With outlier landmarks is 1270 mm, - Without the outlier landmarks is 16 mm	N/A
(Zhu et al., 2011)	Camera + LiDAR	Use of precise 3D Li-dar range fused with a multi-stereo based visual odometry system to detect landmarks	Indoor	A segway robotic platform (RMP400)	Position Error is in range ± 150 mm	Min of angular upper bounds Error : -Stereo is 0.11 deg, -Lidar is 0.11 deg
(Emter and Ulrich, 2012)	Camera + LiDAR	Use a laser scanner (LIDAR) and a camera fusion for simultaneous localization and mapping	Outdoor	Self-developed mobile robot	The system can create maps, as shown in Fig. 6-8	N/A
(Shim and Cho, 2015)	Camera	Robot 2D localization using visual information from the external multi surveillance cameras installed indoors	Indoor	Indoor with a self-developed mobile robot with omnidirectional wheels	Position Error of two-dimensional map is within 71 mm	N/A
(Shalal et al., 2015b)	Camera + Laser scanner + IMU + Odometers	Localization using Extended Kalman Filter for a camera and laser scanner data fusion	Outdoor	CoroWare Explorer platform with on-board sensors	The average of position Error RMS is 103 mm	The average heading Error RMS is 3.32 deg

Author	Sensors	Strategies	Application	Experimental	Position Accuracy (mm)	Orientation Accuracy (deg)
(Nilwong et al., 2019)	Camera + Compass	Comparisons between localization results of Faster Regional-Convolutional Neural Network (Faster R-CNN) landmark detection, and a single convolutional neural network (CNN) to determine the location and compass orientation from the whole image	Outdoor with light source	Wheelchair robot equipped with sensors	Position Error Std: - Faster R-CNN is 1429.9 mm, - CNN is 2097.1 mm, - CNN (AlexNet) is 1546.4 mm	Heading Error Std: - Faster R-CNN is 6.0188 deg, - CNN is 4.7458 deg, - CNN (AlexNet) is 4.9254 deg
(Nemec et al., 2019)	Camera + Odometers + IMU	Sensor fusion between odometers, gyroscope, accelerometer, magnetometer and visual landmark localization system using extended Kalman filter	Indoor	E-puck robot and visual landmark	Position Error RMS < 5mm	N/A

This research incorporates a laser range finder as the primary measure equipment. A laser range finder, utilizing time-of-flight measurement of travel laser, has accuracy within 20 mm (Larsson et al., 1996) depending on the surrounding environment. Therefore, a review on localization using laser with sensors fusion in table 2.6 is necessary for the research. There are many types of sensor fusion with a laser range finder. Laser + Photodiode presented by Souvestre et al. (2009) gives a dynamic precision in 1-6 mm and a static precision in the mm range.

Table 2.6

Review on Localization by using Laser with Sensors Fusion

Author	Sensors	Strategies	Application	Experimental	Position Accuracy (mm)	Orientation Accuracy (deg)
(Larsson et al., 1996)	Laser range finder + Odometer	Localization and mapping using laser range finder and odometer with the range weighted Hough transform (RWHT) algorithm extract lines from the range data	Indoor simulation and a mobile robot	Self-testing system	Position Error SD is 20 mm	Orientation Error is 0.3 deg
(Bento et al., 2005)	Laser range finder + encoder + magnetic sensor	A guidance system for autonomous vehicles navigation in semi-structured outdoor environments using encoders, landmark, and magnetic sensing fusion by EKF	Simulation and real outdoor experiments	Four-wheels actuated electric vehicle ("Robucar")	The results of map plotting in a field and simulation are shown in Fig.6-7. Error SD: -Room size is 15 mm, -Room angle is 0.17 deg	N/A
(Souvestre et al., 2009)	Laser + Photodiode	Using eight beams laser tracking with photodiode sensors, Tilt-Pan is controlled PID control	2D Indoor / Outdoor	A self-laser tracking system prototype	- Static precision is in mm range, - Dynamic precision is in the range 1-6 mm	N/A
(Her et al., 2012)	Laser range finder + IR landmark	Mobile robot localization and mapping using laser range finder and IR landmark camera fusion	Indoor	Self-developed mobile robot	Position Error SD: - X is 83 mm, - Y is 93 mm	Heading Error SD is 1.2 deg
(Canedo-Rodríguez et al., 2016)	Laser range finder + WiFi + Compass + Camera	Multi-sensor fusion algorithm based on particle filters, a laser range finder, a WiFi card, a magnetic compass, and an external multi-camera network	Indoor	Prepared zone with pieces of equipment	Position Error SD of Position (W+C+c) is 880 mm	Heading Error SD of (L+W+C+c) is 0.19 deg
(Le et al., 2019)	LiDAR + IMU	3D Mapping, light laser detection and ranging (LiDAR), and IMU for state estimation, localization, and mapping in the agricultural domain	Outdoor	Both simulate robot and actual four wheels robot	Relative position Error in translation max is 300 mm	Relative heading Error of Rotation (Yaw) < 3 deg

Author	Sensors	Strategies	Application	Experimental	Position Accuracy (mm)	Orientation Accuracy (deg)
(Moreira et al., 2020)	Laser beacon	Laser beacons based systems and natural landmarks by extended Kalman Filters measure its distance and angle in a local referential frame to calculate the angle	The system needs external laser beacons	Simulation and real testing	N/A	Heading Error: - without Kalman filter is 28.64 deg, - with Kalman filter is 0 deg

Some researchers had applied other sensors for localization, as shown in Table 2.7. The correct trajectory's position error for Ultrasonic + Odometer is less than 200 mm (Hoppenot and Colle, 1997), while position RMSE of radar array is 300 mm (Guan et al., 2018). Heading is also measured by radar array with RMSE heading accuracy of 5.73 deg. The magnetic sensor is also studied in position measurement; the mean of position error is 130 mm. In the case of UWB, the average accuracy could reach 200 mm.

Table 2.7

Review on Localization by using Radiofrequency, Magnetic & Light

Author	Sensors	Strategies	Application	Experimental	Position Accuracy (mm)	Orientation Accuracy (deg)
(Hoppenot and Colle, 1997)	Ultrasonic + Odometer	Robot Localization using poor ultrasonic sensors and odometers	Indoor	A robot	Position Error of the corrected trajectory < 200 mm	N/A
(Hsu et al., 2007)	RF + magnetic sensor	Mobile robot localization by Fused Magnetic sensor and received signal strength (RSS) data with Covariance Intersection (CI)	Indoor	Self-developed mobile robot	Mean distance Error: Decreased from 10% to less than 5% Comparing to the localization system only with RSS for estimation	N/A
(Sheinker et al., 2013)	Magnetic sensors	2D localization by detected magnitude and phase of magnetic fields in ULF band (low frequency quasi-static magnetic field)	Outdoor (10m X 11m area)	Simulation and self-testing system on a wheeled cart	Mean Error is 130 mm	N/A
(Guan et al., 2018)	Radar array	Doppler–Azimuth radar array in the framework of nonlinear/non-Gaussian estimation using a particle filter and a random finite set (RFS) model of measurements	Indoor / Outdoor	Simulation	RMSE in position is 300 mm	RMSE Heading is 5.73 deg
(Shi et al., 2020)	UWB	UWB ranging with three transmitters for Automatic Guided Vehicles (AGVs), results are compared with RTK	Indoor / Outdoor	A testing robot platform	Worked in indoor and outdoor area of several hundreds of square meters, - The average Error is about 200 mm, - The Maximum Error is about 400 mm	N/A

Author	Sensors	Strategies	Application	Experimental	Position Accuracy (mm)	Orientation Accuracy (deg)
(De-La-Llana-calvo et al., 2020)	PSD	Finding a robot position by LED emitters are placed on the ceiling in fixed, known positions, a Lens and a Position-Sensitive Detector (PSD) sensor mounted on the top of the robot to detect AOA to calculate the robot's position	Indoor	A testing system	Average positioning Error is49 mm for PSD 4 signals	N/A

2.3 IMU Sensor Fusion for Tilt Measurement

Although most position sensors can report their locations with high accuracy, the orientation is still inadequate for agricultural operation. IMU measures acceleration and angle velocity; the acceleration and angle velocity can fuse by sensor fusion technique to get its angle in roll, pitch, and yaw such as complementary filter, Kalman filter, etc.

2.3.1 Tilt Calculation from IMU Raw Data

Table 2.8 shows the study of IMU for tilts measurement. The accelerometer inside IMU measures the acceleration force vector of gravity, while the gyroscope measures angular velocity. The two pieces of information can be combined with sensor fusion algorithms to accurately determine its tilt.

Table 2.8

Review on Tilts Measurement by IMU and Sensor Fusion

Author	Sensors	Strategies	Application	Experimental	Orientation Accuracy (deg)
(Gui et al., 2015)	IMU	Tilting measurement using Micro-Electro-Mechanical-system (MEMS) based inertial measurement unit (IMU), complementary and Kalman filter	Indoor/Tilt	System tester	The complementary filter can be more stable and accurate than the Kalman filter
(Min and Jeung, 2015)	IMU	Angle Estimation using MEMS gyroscopes and accelerometers by complementary filter compared with cut-off frequency method	Tilt	Self-testing system	RMSE: - Complementary filter is 0.0389 deg, - Cut-off frequency method is 0.0565 deg
(Pititeeraphab et al., 2016)	IMU	Design a tilt measurement by using IMU raw data filtered with average filter and then compare with complementary filter and Kalman filter to get the effectiveness	Indoor/Tilt	Actual sensor data on the movement of a robot arm and simulation	The average filter can help complementary filter or Kalman filter to reduce vibration to get a good estimation as the results in Fig. 11-14
(Ngo et al., 2017)	IMU	Comparison of complementary filter and Kalman filter for quadrotor	Outdoor/Tilt	Simulation and real quadrotor	The complementary filter is more superior to the Kalman filter, drift phenomenon (approximate +-0.5 deg)
(Weng et al., 2017)	IMU	Wireless tilt measurement system using three MEMS accelerometers using Kalman Filter (KF)	Only 1 axis tilt measurement	A prototype testing system	Measuring resolution 0.02 deg, tilt measurement error < 0.004 deg for the step change of 0.05 deg
(Zhe et al., 2020)	IMU	Fusion of the MEMS accelerometer and the MEMS gyroscope by adaptive sparse interpolation lossless complementary filter (ASICF)	Roll and pitch	A self-driving car and the human pose	RMS Error: - Roll is 2.271 deg - pitch is 1.7761 deg

2.3.2 Sensor Fusion for Orientation

The sensor fusion algorithms in Table 2.8 reported that the complementary filter could be more robust and reliable than the Kalman filter (Gui et al., 2015; Ngo et al., 2017). The complementary filter is also shown to be more accurate than the Cut-off frequency method (Min and Jeung, 2015). Weng et al. (2017) reported a tilt measurement system using three MEMS accelerometers with Kalman Filter (KF), gives measuring resolution 0.02 deg, and tilt measurement error < 0.004 deg for the step change of 0.05 deg.

2.4 Chapter Summary

No sensor can measure the position and orientation of an object at the same time. Multi-sensor fusion is a solution to produce high accuracy and precision for localization.

CHAPTER 3
METHODOLOGY

The IMU-coupled TLG system consists of a base station mounted with a laser-pointing unit (LPU) and a mobile unit with a laser-target unit (LTU). The LPU consists of two laser pointers with different wave ranges and a laser rangefinder module. The LTU consists of three laser targets: two projection targets to detect the projected laser pointers and one target to reflect the laser rangefinder from the LPU. The high accuracy and precision of localization are achieved by the innovative design of interaction between the LPU and LTU which is briefly described as follows:

1. The LPU is controlled to point at the middle of the LTU while the LTU is controlled so that the laser targets are perpendicular to the laser-pointing beams.
2. The interactive controlling of the LPU and LTU is achieved by analyzing the projected positions of the LPU's laser pointers on the LTU's projection targets via image processing.
3. With the LPU pointing perpendicularly at the center of the LTU, the position and heading of the mobile unit relative to the laser base station can be accurately and precisely determined using the distance measured by the laser rangefinder, the fanning angle of LPU, and the relative heading angle of the LTU.

The IMU-coupled TLG system demonstrated in this study consists of a laser base station and a mobile unit, as shown in Figure 3.1. Computer software is used for data recording, manual control, and PID setup for both the base station and the mobile unit.

Figure 3.1

IMU-Coupled TLG System

3.1 Laser Base Station

The laser base station comprises a base frame, a laser-pointing unit (LPU), and a fanning-vertical control unit (FVCU), as shown in Figure 3.2. The base frame is constructed as a rectangular box frame with dimensions of 30 cm in width, 50 cm in length, and 110 cm in height, using hollow steel bars. Four level-adjusting poles are applied as the base frame's legs. The LPU is mounted onto FVCU. Then the LPU-FVCU assembly is installed onto the base frame. The FVCU is employed to control the vertical position along the Z-axis and fanning angle in the XY-plane of the LPU.

Figure 3.2

Schematic Illustration of the Laser Base Station

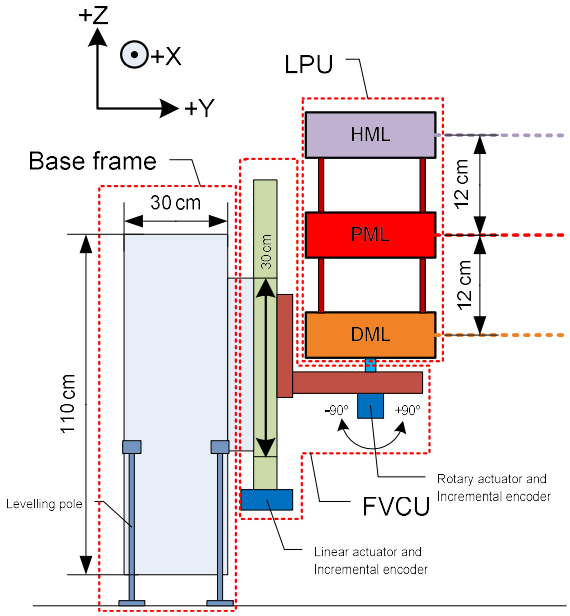

The LPU is designed to track the position and control the heading of the mobile unit. The LPU holds three lasers: a heading-measuring laser (HML), a position-measuring laser (PML), and a distance-measuring laser (DML). The HML, the PML, and the DML are at the top, in the middle, and at the bottom position of the LPU, respectively, with a 12-cm vertical separation. The lasers are situated to point in the same direction and parallel to the ground. A 405-nm violet laser pointer, a 650-nm red laser pointer, and a 650-nm red laser rangefinder are applied as the HML, the PML, and the DML, respectively.

The FVCU, devised to track and control the linear and fanning motions of the LPU, consists of a rotary actuator and a linear actuator (Figure 3.2). The rotary actuator employs a micro-stepping motor and an incremental encoder with a maximum angle of rotation of 180° and a rotating resolution of 9.38×10^{-3} °/step. The linear actuator is driven by a DC motor and controls its moving arm position using an incremental encoder and PID position control with the maximum moving distance of 30 cm. In the FVCU, the rotatory actuator is attached to the moving arm of the linear actuator. It

is oriented so that its plane of rotation is perpendicular to the linear actuator's uniaxial motion.

To allow vertical control along the Z-axis and fanning control in the XY-plane of the LPU, the LPU is attached to the rotary actuator of the FVCU, and then the LPU-FVCU assembly is secured on the base frame so that the linear actuator of the FVCU is in the vertical position. A microcontroller unit (MCU) is employed to process the data from the FVCU and the LPU, to control the actuators in the FVCU, and to remotely communicate the data via 433-MHz radio frequency (RF).

3.2 Mobile Unit

The mobile unit consists of a skid-steering robot, a laser-target unit (LTU), a heading control unit (HCU), and an attitude-measuring unit (AMU), as illustrated in Figure 3.3. The skid-steering robot is a four-wheel-drive using four 24-volt DC motors with H-bridge PWM drivers controlled by an MCU. Skid-steering principal, a typical maneuver for vehicles with non-orientable wheels, controls the mobile unit rotation by applying a speed difference on the left and right wheels, creating lateral slippage or skidding. The skid-steering robot's commands from an external host are remotely transmitted to the MCU via 433-MHz RF. The robot's frame dimensions are 50 cm in width, 70 cm in length, and 140 cm in height, and the size of the wheels is 20.4 cm in diameter. The robot's maximum speed is set at 1.5 m/s.

Figure 3.3

Schematic Illustration of the Mobile Unit

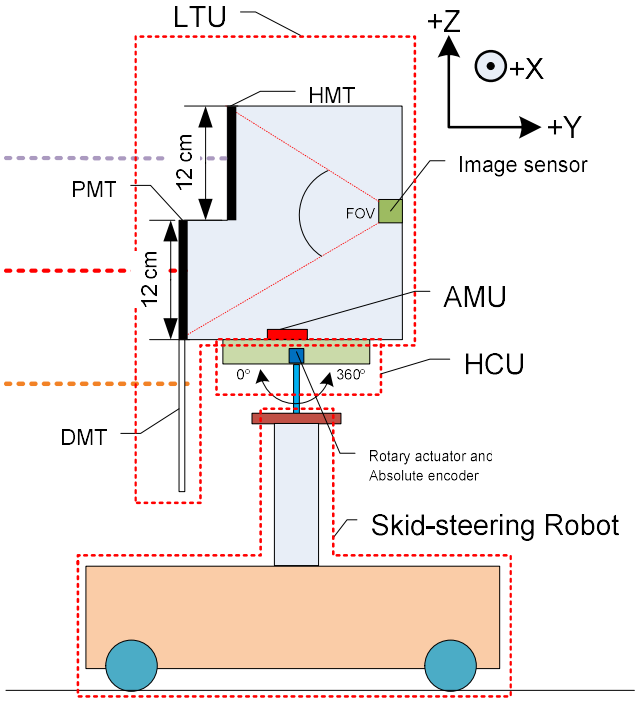

The LTU includes a heading-measuring target (HMT), a position-measuring target (PMT), a distance-measuring target (DMT), and an image sensor. The HMT and the PMT, assigned to project the HML and the PML for heading control and measurement, are 12 cm x 50 cm projector screens made from black, translucent paper. The DMT, assigned to reflect the DML for distance measurement, is a 12 cm x 50 cm laser reflecting screen made from a white, opaque plastic sheet. The HMT, the PMT, and the DMT are placed at the top, in the middle, and at the bottom position of the LTU, respectively, with a 12-cm vertical separation between their centers. The image sensor used to detect and determine the positions of the projected HML and PML on the HMT's and PMT's screens is a Pixy2 CMUcam5 smart camera with a frame rate of 60 frames per second and the field of view (FOV) covering both HMT and PMT. The HMT, the PMT, and the image sensor are placed in a dark enclosure, where the HMT and the PMT are placed in front of the image sensor at 18 cm and 30 cm away, respectively.

The positions of the projected HML on the HMT and the projected PML on the PMT are used to control the LPU and LTU so that the lasers perpendicularly pointing at the center of their assigned targets. This is critical for the IMU-coupled TLG system to achieve the highest accuracy and precision in localization and is elaborated in further detail in Control Description. The Pixy2 smart camera is programmed to find a violet laser blob from the HML on the HMT and a red laser blob from the PML on the PMT. The centroids of the area of these laser blobs are then quantified via image processing of the Pixy2 smart camera and reported to the microcontroller as the positions of the projected lasers. To avoid interference for the image sensor's detection of projected HML and PML, the maximum light intensity allowed on the HMT and the PMT is 20,000 lux.

The HCU is a 360° bidirectional, rotatable stand. A DC-motor rotary actuator with PID position control drives and controls its rotational motion and an absolute encoder measures its angle of rotation. For attitude (roll and pitch tilts) measurement, the AMU utilizes a low-cost 6DoF IMU where roll and pitch are computed using IMU sensor fusion with complementary filter (Gui et al., 2015; Min and Jeung, 2015; Ngo et al., 2017).

For the complete assembly of the mobile unit, the HCU is secured on top and at the center of the robot's frame. The LTU and AMU are then placed and centered on the HCU, allowing 360° rotation of the LTU and the AMU on the mobile unit. An MCU is utilized to process the data from the LTU, the HCU, and the AMU, control the rotary actuator in the HCU, and remotely communicate the data via 433-MHz RF.

3.3 System Cost Breakdown

The IMU-coupled TLG system's total cost mainly comes from the structural, mechanical, electronic components of three hardware groups: the laser base station, the mobile unit, and the wireless communication components. The cost breakdown was based on retail and online prices plus shipping for Bangkok, Thailand, in February 2021 and is summarized in Table 3.1. The total cost of the IMU-coupled TLG system for this study was $950 in USD. It is to be noted that the skid-steering robot's cost is not included since its purpose in this study was only to be a model rover for demonstrating the performance of the IMU-coupled TLG system.

Table 3.1

Cost Breakdown of the IMU-Coupled TLG System (based on Retail and Online Prices plus Shipping for Bangkok, Thailand in February 2021)

Hardware Group	Subgroup	Component Descriptions	Cost in USD
Laser Base Station	Base Frame	Materials and fabrication	$150.00
	Laser-pointing Unit (LPU)	50-meter laser rangefinder module – 1 unit	$90.00
		405-nm violet laser pointer – 1 unit	$20.00
		605-nm red laser pointer – 1 unit	$10.00
		OMRON E6B2-CWZ6C rotary encoder– 2 units	$70.00
	Fanning-vertical Control Unit (FVCU)	DRV8825 stepper motor driver – 1 unit	$10.00
		Rtelligent Nema 17 stepper motor – 1 unit	$20.00
		Linear Actuator – 1 unit	$70.00
		STM32F3 Discovery microcontroller – 1 unit	$20.00
		Circuit components	$50.00
Mobile Unit	Laser-target Unit (LTU)	Structural frame – materials and fabrication	$100.00
		Pixy 2 CMUcam5 image sensor – 1 unit	$150.00
	Heading Control Unit (HCU)	DC-geared motor – 1 unit	$15.00
		L298N H-Bridge DC-motor driver – 1 unit	$10.00
		5V 1024-pulse absolute encoder– 1 unit	$50.00
		Circuit components	$50.00
		Battery – 1 unit	$25.00
	Attitude-measuring Unit (AMU)	IMU with STM32F3 Discovery microcontroller	$20.00
Wireless Communication	Wireless Transceivers	433-MHz radio frequency (RF) modules – 8 units	$20.00
Estimated Total			$950.00

3.4 Input Parameters

The input parameters for determining the robot's position and orientation (attitude and heading) in the IMU-couple TLG system, assuming that both the LPU and LTU are correctly and promptly controlled as elaborated in Control Descriptions, are described as follows:

1) The distance between the LPU and the LTU (r) measured by the DML on the LPU at the laser base station (see Figure 3.4)
2) The fanning angle of the LPU (β) measured by the FVCU at the laser base station (see Figure 3.4)
3) The height of the LPU (h) measured by the FVCU at the laser base station
4) The roll tilt of the LTU (θ) measured by the AMU on the mobile unit
5) The pitch tilt of the LTU (ϕ) measured by the AMU on the mobile unit

6) The relative heading angle between the LTU and the skid-steering robot (γ) measured by the HCU on the mobile unit
7) The robot's heading on the field (α) is the sum of β and γ

Figure 3.4

Working Field and Reference Axes

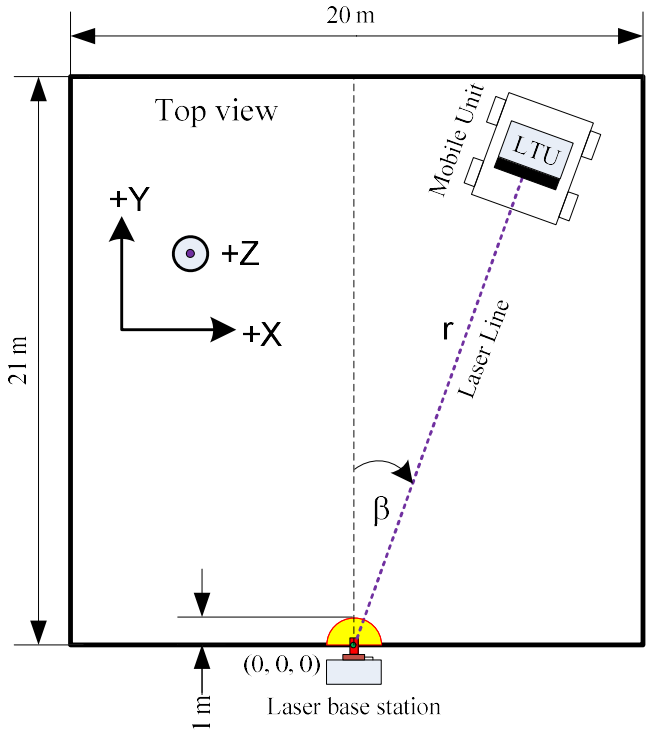

3.5 Control Descriptions

In the IMU-coupled TLG system, the robot's position and heading are computed using the distance between the LPU and LTU and the height and fanning angle of the LPU, which is further elaborated in Determination of Robot's Position and Orientation. For the highest accuracy of distance and heading measurements, the lasers, namely the HML, the PML, and the DML, must be parallel to the ground and perpendicularly pointing at the center of their assigned targets, the HMT, the PMT, and the DMT, respectively. Hence, the LPU on the laser base station and the LTU on the mobile unit must be simultaneously controlled as follows:

3.5.1 Fanning Angle and Height Control of the LPU

The LPU control, carried out by the FVCU, aims to keep its lasers' projection at the center of their assigned targets. Since the HML, the PML, and the DML are all on the same LPU's rigid body and positioned with the same vertical separation as the centers of their assigned targets on the LTU, the LPU control is solely focused on maintaining the projected PML position at the center of the PMT. If the PML points perpendicularly to but away from the center of the PMT, it yields center-deviated distances of the projected PML in both X- and Z-axes of the PMT, designated as Err_X^{PMT} and Err_Z^{PMT}, respectively, as illustrated in Figure 3.5(a). To keep the projected PML at the PMT's center, the rotary actuator in the FVCU controls the fanning angle (β) of the LPU to minimize the Err_X^{PMT} to zero, while the linear actuator in the FVCU controls the height (h) of the LPU to minimize the Err_Z^{PMT} to zero, as depicted in Figure 3.5(b). The LPU fanning angle and height control for Err_X^{PMT} and Err_Z^{PMT} minimization is achieved using a PID control with PWM signaling to the FVCU, as illustrated in Figure 3.5(c).

Figure 3.5

LPU Control Maintaining the Projected PML at the Center of the PMT: (a) Before LPU Control, Center-Deviated PML Projection on the PMT (b) After LPU Control, PML Projection at the PMT's Center (c) LPU Fanning Angle and Height Control Strategy

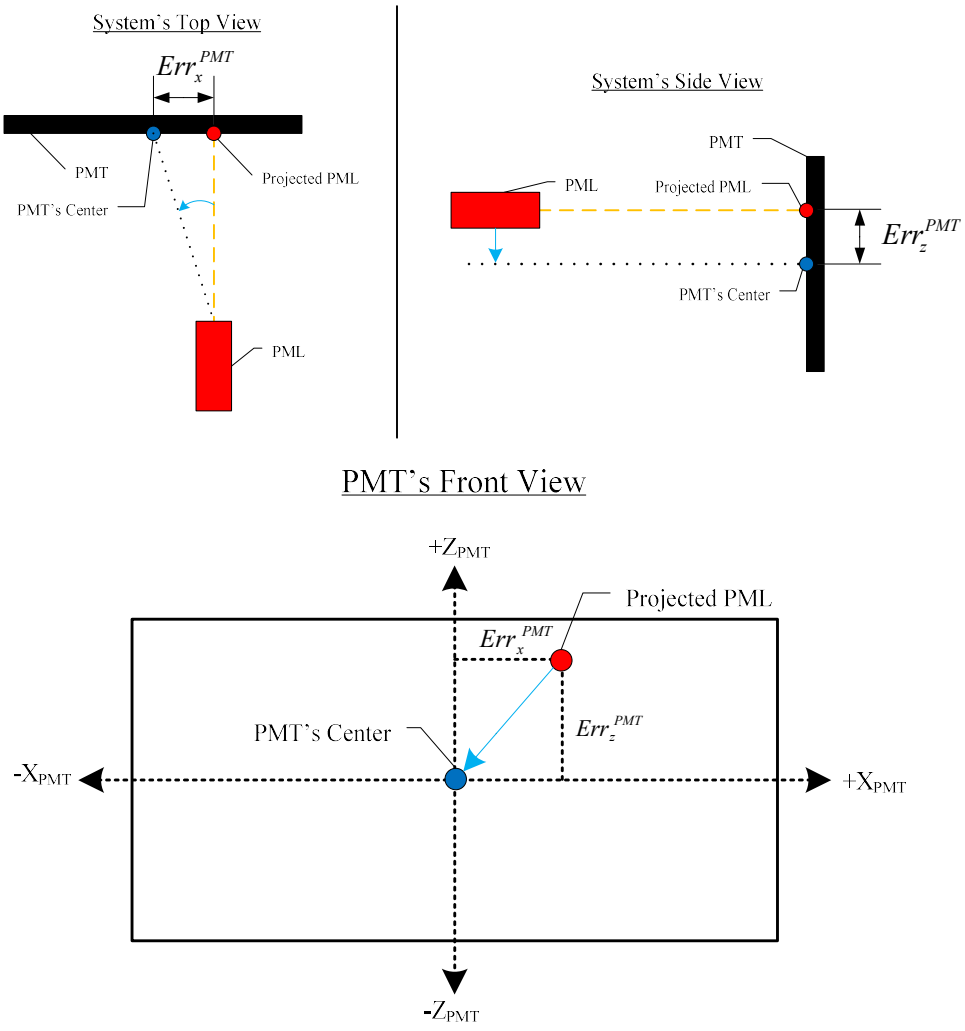

(a)

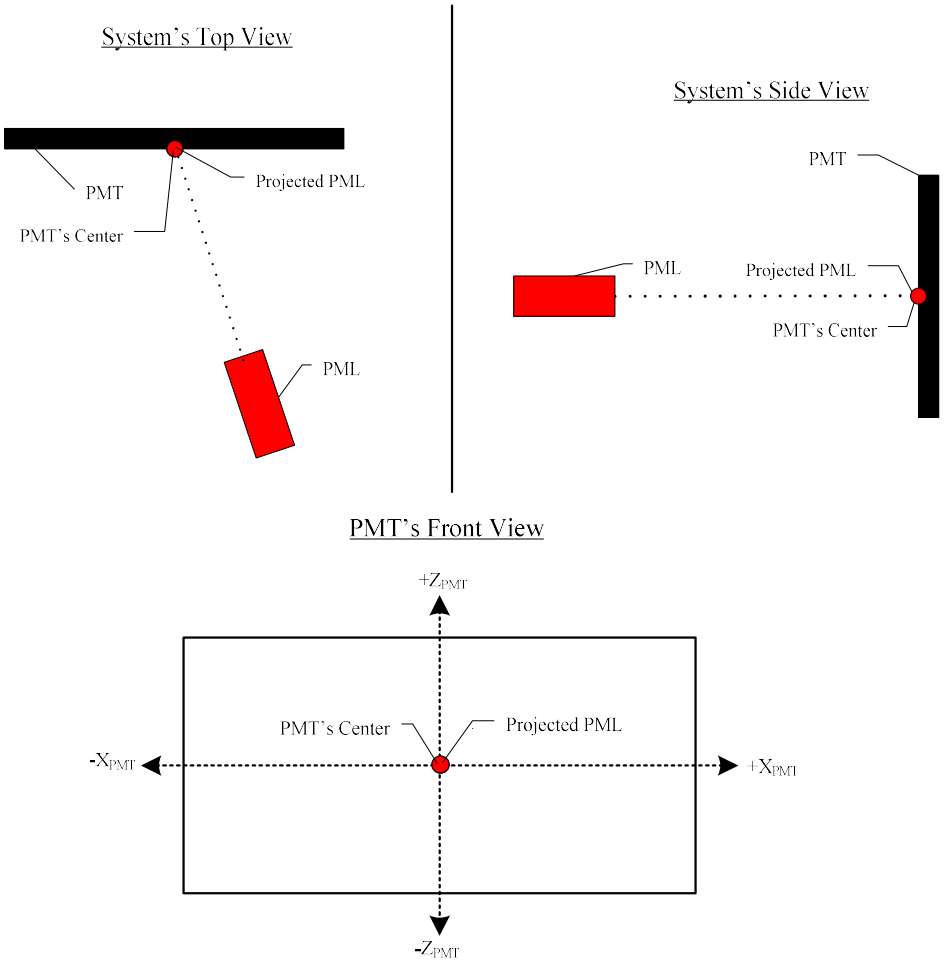
System's Top View
PMT
Projected PML
PMT's Center
PML
System's Side View
PMT
PML
Projected PML
PMT's Center
PMT's Front View
+Z_PMT
PMT's Center
Projected PML
-X_PMT
+X_PMT
-Z_PMT

(b)

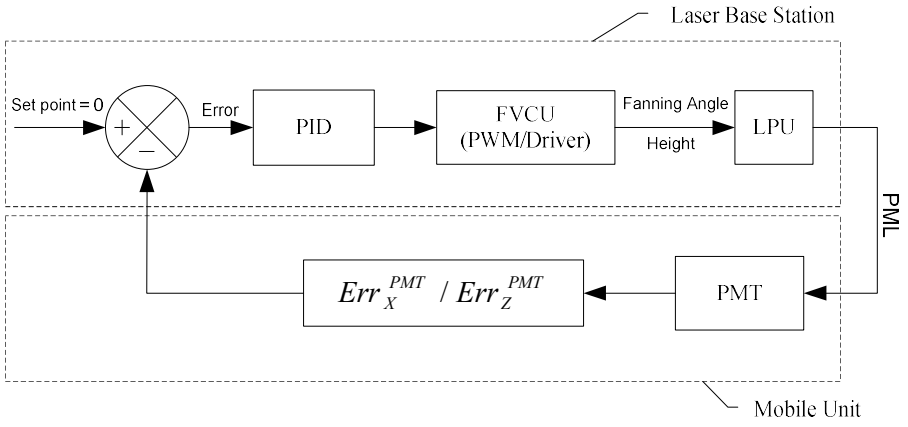
Laser Base Station
Set point = 0
Error
PID
FVCU
(PWM/Driver)
Fanning Angle
Height
LPU
PML
Err X PMT / Err Z PMT
PMT
Mobile Unit

(c)

3.5.2 Heading Control of the LTU

The aim of the LTU's heading control carried out by the HCU is to ensure that three lasers' beams from the LPU are perpendicular to the targets of the LTU. Suppose the LPU's laser beams are non-perpendicular to the LTU's targets' screens. In that case, there is a difference in the center-deviated distances along the X-axis of the targets between the projected HML on the HMT (Err_X^{HMT}) and the projected PML on the PMT (Err_X^{PMT}), as shown in Figure 3.6(a). The magnitude of the difference between Err_X^{HMT} and Err_X^{PMT} , designated as ΔErr_X , is defined as follows:

$$\Delta Err_x = \left| Err_X^{HMT} - Err_X^{PMT} \right| \tag{1}$$

If $\Delta Err_X > 0$, the rotary actuator in HCU rotates the heading of LTU to minimize ΔErr_X to zero, confirming the laser beams' perpendicularity from the LPU to the LTU's targets, as illustrated in Figure 3.6(b). The LTU heading control for ΔErr_X minimization is achieved using a PID control with PWM signaling to the HCU, as illustrated in Figure 3.6(c).

Figure 3.6

LTU Control Maintaining the Perpendicularity of the Lasers' Beams from the LPU to the LTU's Targets: (a) Before LTU Control, Non-perpendicular Lasers' Beams to Targets (b) After LTU Control, Perpendicular Lasers' Beams to Targets (c) LTU Heading Control

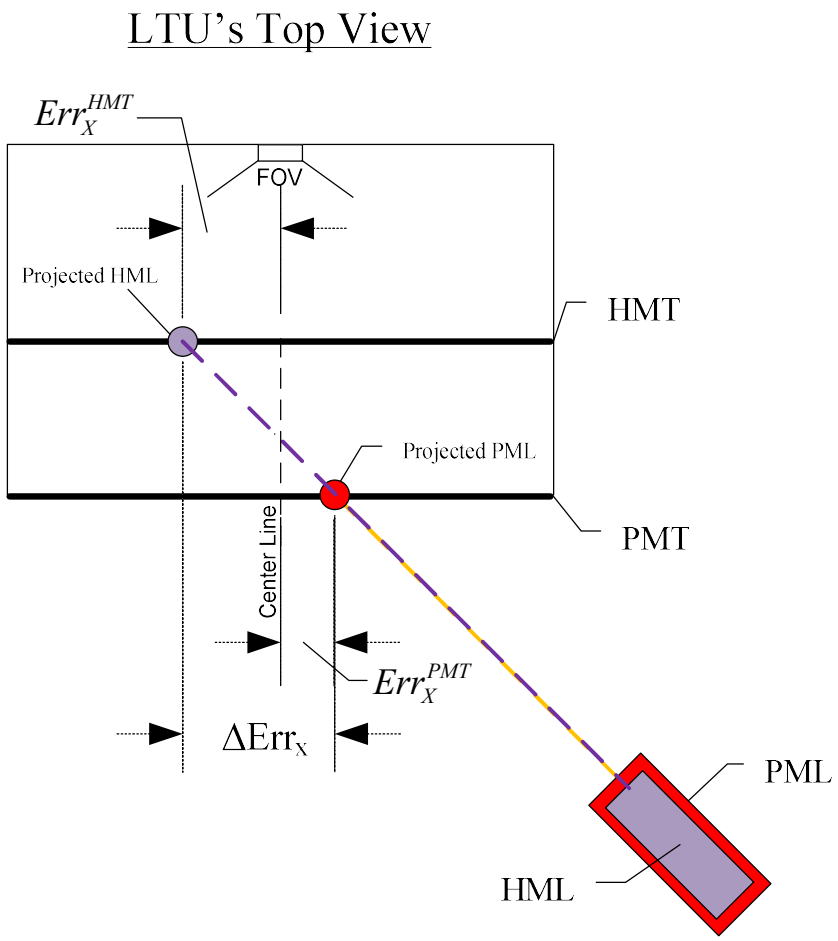

(a)

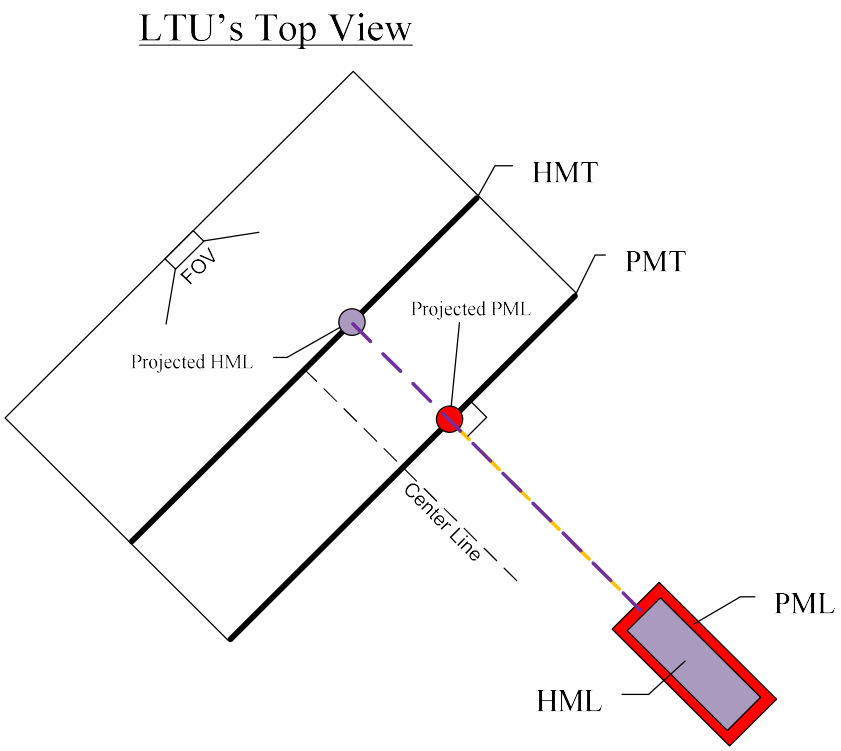

(b)

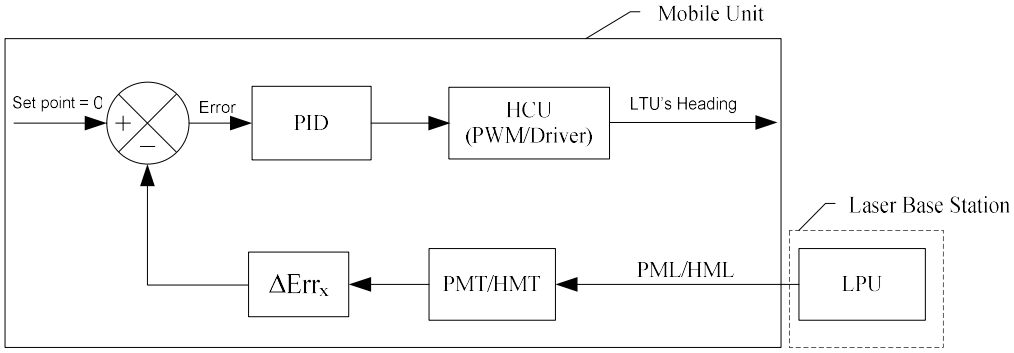

(c)

3.6 Determination of Robot's Position and Orientation

Assuming the perpendicularity and centering of the lasers' projections on the targets as described in Control Description, the robot's position and heading in Figure 3.7 can be accurately determined as follows:

$$X = r \sin \beta \tag{2}$$

$$Y = r \cos \beta \tag{3}$$

$$Z = h \tag{4}$$

$$Heading(\alpha) = \beta + \gamma \tag{5}$$

The robot's roll (θ) and pitch (ϕ) tilts are calculated via sensor fusion of low-frequency signals from a triple-axis accelerometer and high-frequency signals from a triple-axis gyroscope of a low-cost 6DoF IMU in the AMU through complementary filter (Gui et al., 2015; Ngo et al., 2017).

Figure 3.7

Schematic Drawing of the IMU-Coupled TLG System for the Determination of the Robot's Position and Heading

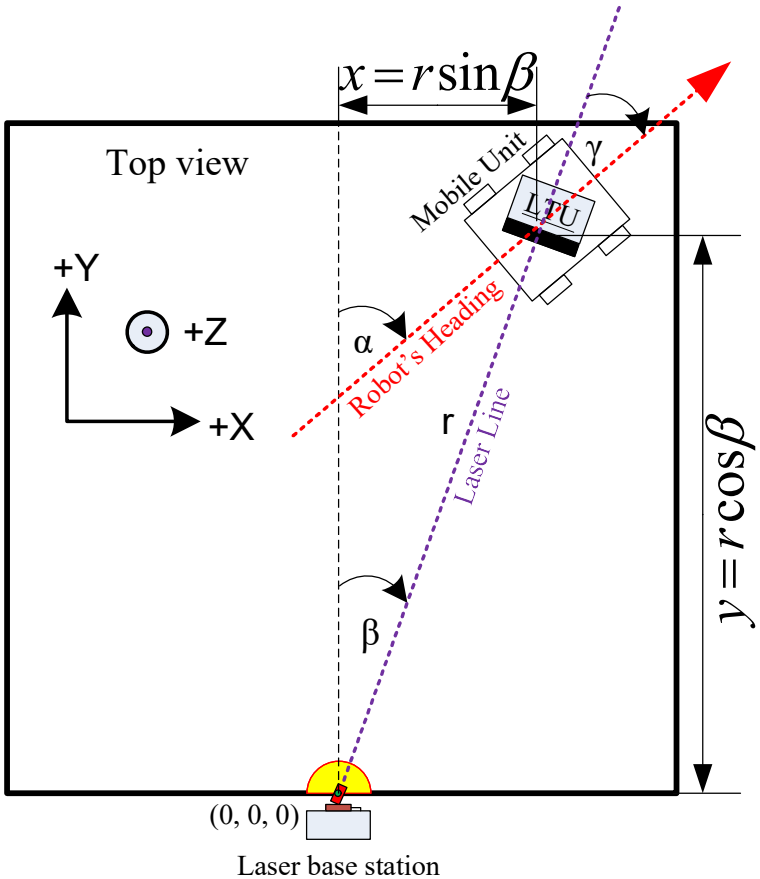

3.7 Data Flow and Communication Diagram

In the IMU-coupled TLG system, the laser base station, the mobile unit, and the computer communicate data among themselves with a sampling rate of 100 ms, as depicted in Figure 3.8. The communication is carried out using HC-11 wireless transceiver modules with a frequency band of 433 MHz. For all transceiver modules, the RF power is set to 10 dBm with the data baud rate of 115,200 bps and the transmission delay time of 10 ms. The operating distance of these communication modules is approximately 30 m.

Figure 3.8

Data Flow and Communication Diagram

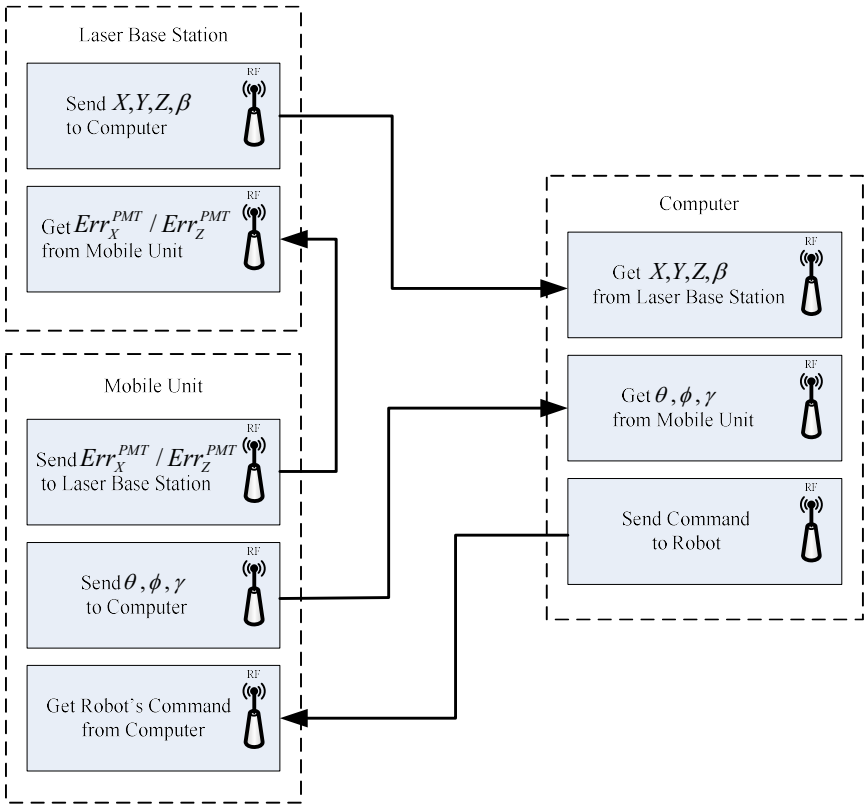

3.8 Chapter Summary

The system in this chapter describes the mobile unit and the laser base unit. Robot 2D location (X, Y) comes from the distance and relative facing angles between the mobile and laser base units, with a condition that the LPU must always be controlled to remain orthogonal to the laser targets on the LTU via PID position controller. Robot height (Z) is measured and controlled from an encoder at the bottom of the laser pole installed on the base unit. Robot attitude (heading, roll, and pitch) is measured via AMU mounted on the LTU of the mobile unit. Error signals and measurement values communicate between the modules via radio frequency (RF).

CHAPTER 4
EXPERIMENTAL RESULTS

The experiments aim to demonstrate that the TLG system can properly operate in an outdoor environment within its limitations. An actual flat field and paddy field were designed to test for getting position and orientation error to answer the developed system can work or not for automatic guidance farming depend on the robot location and pose accuracy. Field design and system preparation are elaborated in this chapter along with methodology and data processing.

4.1 Field and Measurement Design

The distance measuring by a laser range finder is limited to 25 m because the system needs a range accuracy less than 2 cm under the intensity of sunlight. Therefore, the working field was 20 m X 20 m for both the flat and paddy area. In technical terms, the laser range finder cannot measure in a short-range between 0-1 m; so, the laser base station needs to move back for 1 m, as shown in Figure 4.1.

4.1.1 Working Field and Reference Axes

An operational area for the mobile unit is a 20 m x 21 m rectangular plain with its reference axes, designated as X, Y, and Z, defined concerning the laser base station, as depicted in Figure 3.4. The origin of the working field (0, 0, 0) is assigned as the LPU's position points at the laser base station. Due to the DML's low measurement accuracy at a close distance to the target, the working field excludes a semicircular area with a radius of 1 m around the laser base station.

4.1.2 Method for System Demonstration

The operation of a high-accuracy, position-aware robot using the IMU-coupled TLG system was demonstrated in an outdoor setting on a 20 m x 21 m treeless, flat field, and paddy field, as depicted in Figure 3.4. The robot was manually remote controlled to move along a predetermined path on the area from the numbered location 1 to 10, as shown in Figure 4.1, without exceeding the maximum speed of 1.2 m/s.

Figure 4.1

Field and Designed Path for the System Demonstration and for the Determination of Position/Orientation Accuracy and Precision

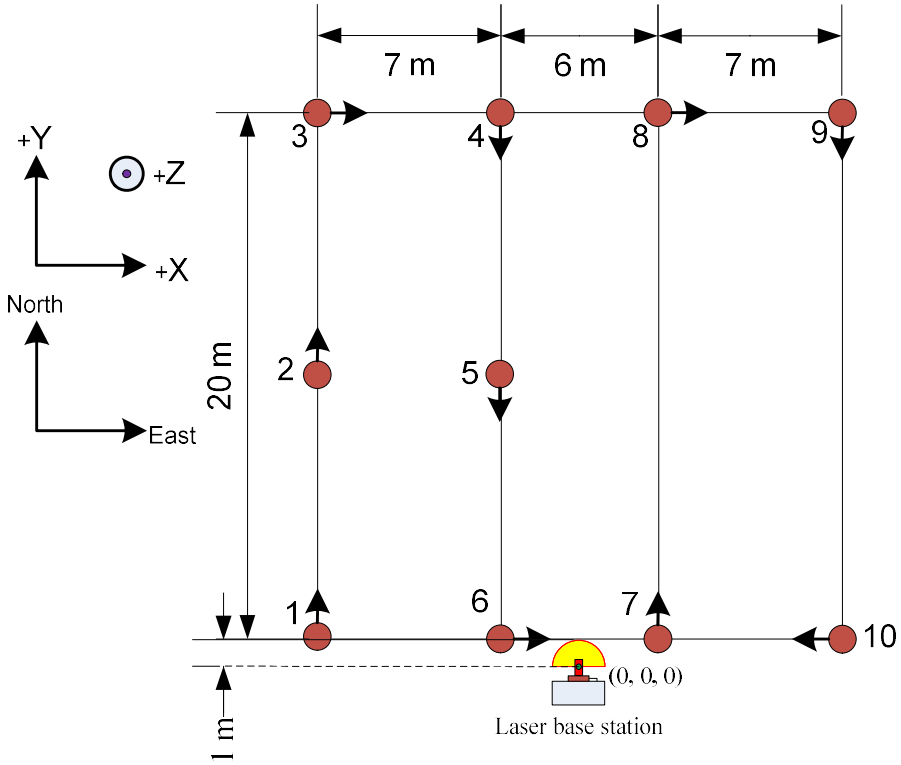

The robot's heading was preassigned at the numbered locations with a designated arrow. At each numbered location, the robot was stopped to physically verify its actual position (XYZ coordinates) and angles of orientation on the field. The reported values from the IMU-coupled TLG system were recorded. The light intensity on the laser targets, HMT and PMT, was also noted at each numbered location. Furthermore, both systems recorded the robot's XY position every second to generate its horizontal trajectory on the designed path. To validate the system's outdoor capability in daylight and ensure the stringency of the statistical analysis, the system demonstration was repeated five to ten times at each numbered location under various light intensities on the field ranging from 45,000 lux to 85,000 lux during the daytime.

The robot's actual position and orientation ($\hat{R}_i$) at the l^{th} location is defined as:

$$\hat{R}_l = (\hat{X}_l, \hat{Y}_l, \hat{Z}_l, \hat{\alpha}_l, \hat{\theta}_l, \hat{\phi}_l) \tag{6}$$

The system's reported (R_{li}) position and orientation of i^{th} epoch at the l^{th} location is defined as:

$$R_{li} = (X_{li}, Y_{li}, Z_{li}, \alpha_{li}, \theta_{li}, \phi_{li}) \tag{7}$$

The system's average reported position and orientation ($\bar{R}_l$) and the standard deviation (σ_l) at the l^{th} location are computed as follows:

$$\bar{R}_l = \frac{1}{N_l} \sum_{i=1}^{N_l} R_{li} \tag{8}$$

Where N_l is the total number of epochs at the l^{th} location.

$$\sigma_l = \sqrt{\frac{1}{N_l - 1} \sum_{i=1}^{N_l} (R_{li} - \bar{R}_l)^2} \tag{9}$$

The system's position and orientation accuracy (A_l) at each numbered location are reported as the absolute difference between the robot's actual position and orientation ($\hat{R}_l$) and the system's average reported values ($\bar{R}_l$), which can be expressed as:

$$A_l = \left| \bar{R}_l - \hat{R}_l \right| \tag{10}$$

By averaging A_l from all numbered location, the overall system's position and orientation accuracy (A_{OA}) can be determined as follows:

$$A_{OA} = \frac{1}{M} \sum_{l=1}^{M} A_l \tag{11}$$

Where M is the total number of the measured locations.

The system's position and orientation precision at each numbered location is reported as the standard deviation (σ_l) of the measurements at that numbered location. The

system's overall position and orientation precision (P_{OA}) are quantified as the combined standard deviation of the system's reported location and orientation at all numbered locations. Since the acquired measurement at each site is independent of one another, the standard deviations were combined using a weighted sum of variance. Hence, the system's P_{OA} is expressed as:

$$P_{OA} = \sqrt{\frac{\sum_{l=1}^{M}(N_l - 1)\sigma_l^2}{\sum_{l=1}^{M}(N_l - 1)}} \tag{12}$$

4.2 Field Experiments

A flat field and an actual paddy are prepared to demonstrate the system. Setting up parameters and field size is the same. The difference is only field type to compare the accuracy of both areas. Distance between the actual positions to ten marked points along the moving path is measured for ten rounds and recorded in a table. Average statistic applied to the raw data for each difference distance as shown in Table 4.1. The most experimental data shown in this section comes from the flat field except in Figure 4.5.

4.2.1 Flat Field Experiments

For the determination of the robot's actual position and orientation, the system's accuracy, and the light intensity on the HMT and the PMT at each numbered location were physically verified and reported, as summarized in Table 4.1.

Table 4.1

The Actual Position and Orientation of the Skid-Steering Robot Physically Verified at Each Numbered Location on the Field

Location (l)	Distance from the laser base station (cm)	Average light intensity on HMT and PMT (lux)	$\hat{X}_l$ (cm)	$\hat{Y}_l$ (cm)	$\hat{Z}_l$ (cm)	$\hat{\alpha}_l$ (º)	$\hat{\theta}_l$ (º)	$\hat{\phi}_l$ (º)
1	1,000	9,266	-1,000	0	0	0	-2	-1
2	1,415	9,416	-1,000	1,000	-1	0	-2	-1
3	2,237	16,462	-1,000	2,000	-2	90	0	-3
4	2,023	9,108	-300	2,000	-1	180	2	2
5	1,045	8,847	-300	1,000	0	180	1	1
6	300	16,563	-300	0	0	90	0	1
7	300	8,918	300	0	1	0	-1	-1
8	2,023	16,752	300	2,000	0	90	-1	0
9	2,237	9,374	1,000	2,000	0	180	0	-2
10	1,000	5,874	1,000	0	2	-90	1	-1

After multiple measurements at each numbered location, the robot's average XYZ coordinates, headings, and attitudes with the computed local accuracy reported by the IMU-coupled TLG system are shown in Table 4.2.

Table 4.2

Average XYZ Coordinates, Headings, and Attitudes of the Robot at Each Numbered Location Reported by the IMU-Coupled TLG System with Computed Local (A_l) and Overall (A_{OA}) Accuracy

Location (l)	X (cm)		Y (cm)		Z (cm)		Heading (º)		Roll (º)		Pitch (º)	
	$\bar{X}_l$	A_l^X	$\bar{Y}_l$	A_l^Y	$\bar{Z}_l$	A_l^Z	$\bar{\alpha}_l$	A_l^α	$\bar{\theta}_l$	A_l^θ	$\bar{\phi}_l$	A_l^ϕ
1	-1,000.67	0.67	0.67	0.67	0.11	0.11	-0.78	0.78	0.33	2.33	0.44	1.44
2	-1,000.78	0.78	1,000.78	0.78	0.00	1.00	0.11	0.11	-0.56	1.44	0.11	1.11
3	-1,001.33	1.33	2,002.00	2.00	-1.22	0.78	89.00	1.00	-0.89	0.89	-3.00	0.00
4	-301.11	1.11	2,002.67	2.67	-0.78	0.22	179.22	0.78	2.44	0.44	2.33	0.33
5	-300.67	0.67	1,001.67	1.67	0.44	0.44	180.00	0.00	0.78	0.22	0.44	0.56
6	-300.33	0.33	0.44	0.44	0.78	0.78	91.33	1.33	0.00	0.00	0.00	1.00
7	300.44	0.44	0.56	0.56	1.56	0.56	1.67	1.67	-0.78	0.22	-0.89	0.11
8	301.11	1.11	2,001.44	1.44	0.33	0.33	88.78	1.22	-0.22	0.78	0.67	0.67
9	1,001.78	1.78	2,001.67	1.67	1.67	1.67	178.89	1.11	1.33	1.33	-1.44	0.56
10	1,001.00	1.00	1.78	1.78	2.00	0.00	-89.00	1.00	1.11	0.11	0.78	1.78
Overall Accuracy	A_{OA}^X = 0.92 cm		A_{OA}^Y = 1.37 cm		A_{OA}^Z = 0.59 cm		A_{OA}^α = 0.90º		A_{OA}^θ = 0.78º		A_{OA}^ϕ = 0.76º	

The overall accuracies for X, Y, Z, α , θ , and ϕ reported by the IMU-coupled TLG system are within 0.92 cm, 1.37 cm, 0.59 cm, 0.90º, 0.78º, and 0.76º, respectively. The local maximum errors and standard deviations at each numbered location reported by the IMU-coupled TLG system are presented in Table 4.3.

Table 4.3

Maximum Errors and Standard Deviations of XYZ Coordinates, Headings, and Attitudes of the Robot Reported by the IMU-Coupled TLG System with Computed Overall Precision (P_{OA})

Location (l)	X (cm)		Y (cm)		Z (cm)		Heading (º)		Roll (º)		Pitch (º)	
	Absolute Maximum Error	σ_l^X	Absolute Maximum Error	σ_l^Y	Absolute Maximum Error	σ_l^Z	Absolute Maximum Error r	σ_l^α	Absolute Maximum Error	σ_l^θ	Absolute Maximum Error	σ_l^ϕ
1	2.00	0.87	2.00	0.71	1.00	0.60	3.00	1.39	2.00	0.87	2.20	0.88
2	3.00	1.09	2.00	0.67	2.00	0.71	1.00	0.60	2.00	0.73	2.00	0.60
3	3.00	1.00	4.00	1.12	1.00	0.44	2.00	1.00	2.00	0.78	1.00	0.50
4	2.00	0.60	4.00	0.87	1.00	0.44	3.00	1.20	1.00	0.53	1.00	0.50
5	2.00	0.71	2.00	0.50	1.00	0.53	0.00	0.00	1.00	0.44	1.00	0.53
6	1.00	0.50	1.00	0.53	2.00	0.83	3.00	1.12	0.00	0.00	1.00	0.00
7	1.00	0.53	1.00	0.53	1.00	0.73	3.00	1.00	1.00	0.67	1.00	0.33
8	2.00	0.78	2.00	0.53	2.00	1.12	3.00	0.83	3.00	1.09	2.00	0.71
9	3.00	0.67	3.00	0.71	2.00	0.50	2.00	0.93	2.00	0.50	2.00	0.73
10	2.00	0.50	2.00	0.44	1.00	0.50	2.00	0.87	2.00	0.93	2.00	0.67
Overall Maximum Error	3.00 cm		4.00 cm		2.00 cm		3.00º		3.00º		2.20º	
Overall Precision	P_{OA}^X = 0.75 cm		P_{OA}^Y = 0.69 cm		P_{OA}^Z = 0.67 cm		P_{OA}^α = 0.96º		P_{OA}^θ = 0.71º		P_{OA}^ϕ = 0.59º	

The overall precisions for X, Y, Z, α , θ , and ϕ reported by the IMU-coupled TLG system are within 0.75 cm, 0.69 cm, 0.67 cm, 0.96º, 0.71º, and 0.59º, respectively. The overall maximum errors for X, Y, Z, α , θ , and ϕ reported by the IMU-coupled TLG system are 3.00 cm, 4.00 cm, 2.00 cm, 3.00º, 3.00º, and 2.20º, respectively. Overall maximum error, accuracy, and precision of the robot's position and orientation reported by the IMU-coupled TLG system are summarized in Table 4.4.

Table 4.4

Summary of Overall Maximum Error, Accuracy, and Precision of the Robot's Position and Orientation Reported by the IMU-Coupled TLG System

Summary	IMU-coupled laser-guided system					
	X (cm)	Y (cm)	Z (cm)	Heading	Roll	Pitch
Overall Maximum Error	3.00	4.00	2.00	3.00º	3.00º	2.20º
Overall Accuracy (A_{OA})	0.92	1.37	0.59	0.90º	0.78º	0.76º
Overall Precision (P_{OA})	0.75	0.69	0.67	0.96º	0.71º	0.59º

Moreover, a multipass, horizontal trajectory of the robot generated by real-time XY position tracking via the IMU-coupled TLG system is depicted in Figure 4.2. Hence, the localization and the horizontal path tracking of the IMU-coupled TLG system were found to be highly accurate and precise all along the designed path.

Figure 4.2

Multipass Trajectories (Solid Green Line) of the Skid-Steering Robot on the Designed Path (Dotted Red Line) Generated by the Real-Time Position Tracking of the IMU-Coupled TLG System in a Flat Field

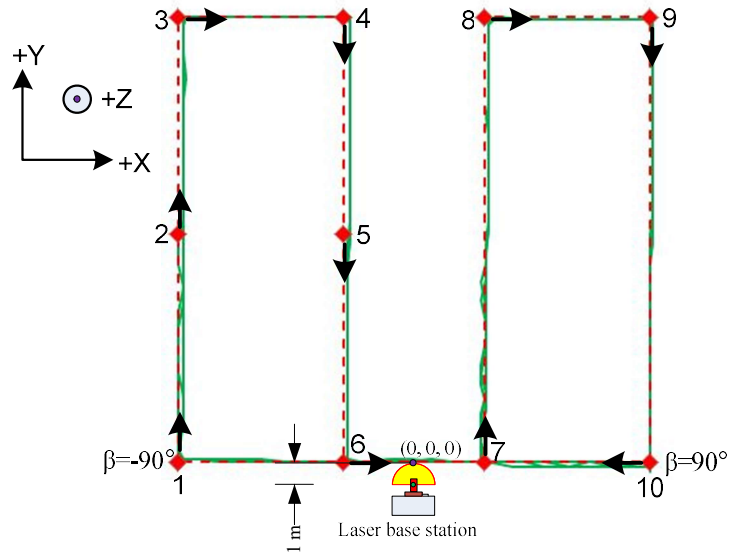

Since the XYZ and heading measurements by the IMU-coupled TLG system solely rely on HML and PML detection accuracy on the HMT and PMT, the laser beam divergence due to its travel distance and sunlight interference could deteriorate the overall accuracy and precision. The local XYZ/heading accuracy and precision at each numbered location were plotted against the mobile unit's distance from the laser base station and the average light intensity on the laser targets. The local XYZ/heading accuracy and precision versus the robot's distance from the laser base at each numbered location are illustrated in Figure 4.3(a)-4.3(d) and Figure 4.3(e)-4.3(h), respectively.

Figure 4.3

The Local Accuracy ( ) and Precision ( ) of the Robot's XYZ Coordinates and Heading Reported by the IMU-Coupled TLG System at the Numbered Locations versus the Mobile Unit's Distance from the Laser Base Station

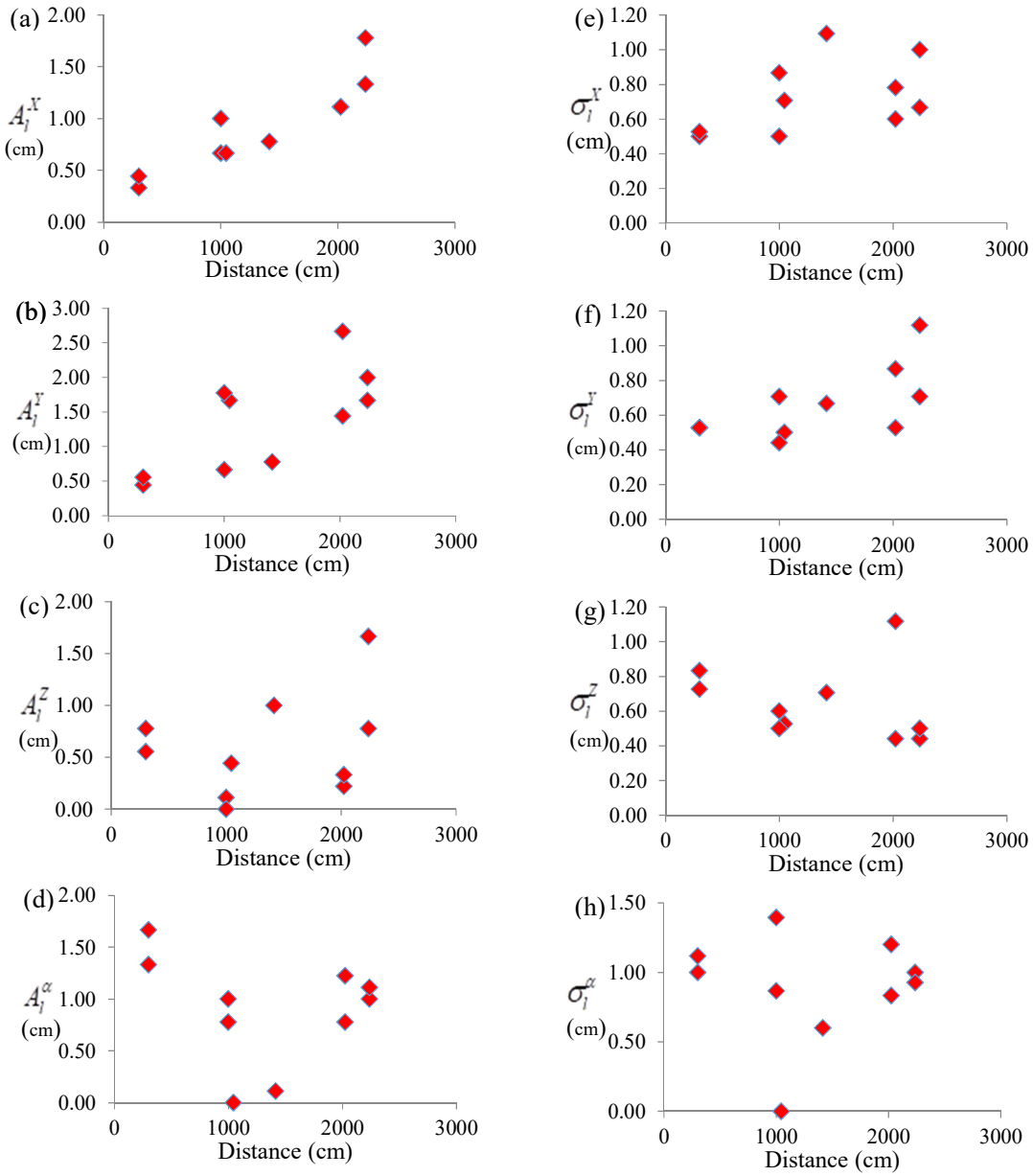

Within the given field size, no correlation between the IMU-coupled TLG system's overall accuracy and precision and the mobile unit's distance from the laser base station was established. The local XYZ/heading accuracy and precision versus the

average light intensity on the laser targets at each numbered location are depicted in Figure 4.4(a)-4.4(d) and Figure 4.4(e)-4.4(h), respectively. If not exceeding 20,000 lux, the varying light intensity on the laser targets during the daytime did not significantly affect the system's overall accuracy and precision.

Figure 4.4

The Local Accuracy (A_l) and Precision (σ_l) of the Robot's XYZ Coordinates and Heading Reported by the IMU-Coupled TLG System at the Numbered Locations versus the Average Light Intensity on the HMT and PMT

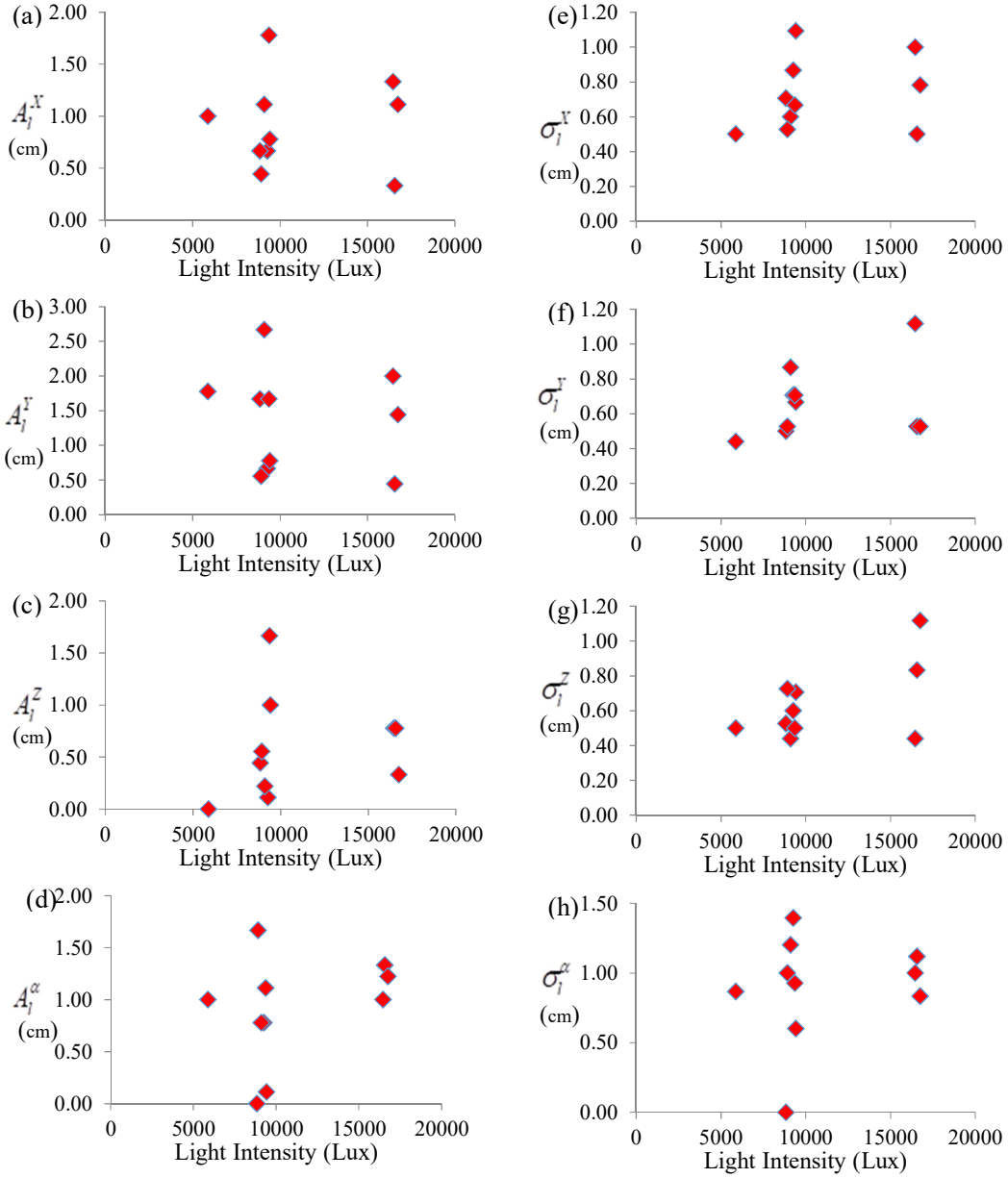

4.2.2 Paddy Field Experiments

The actual paddy field testing is designed to demonstrate the system worked on a rough surface. The experiment was repeated in a dry paddy field in Ratchaburi province, Thailand, with the same conditions as flat-field testing. The result in Figure 4.5 presents a position plot for multipass trajectories moving in the paddy field. The overall position accuracy is 1.72 cm, and the heading error is 1.0 deg. The position error is not significant compare with the position error of flat field testing in Figure 4.4. From Figure 4.5, between point 10 to point 7, there was an uneven area that led to many mistakes in that area.

Figure 4.5

Multipass Trajectories (Solid Green Line) of the Skid-Steering Robot on the Designed Path (Dotted Red Line) Generated by the Real-Time Position Tracking of the IMU-Coupled TLG System in a Paddy Field

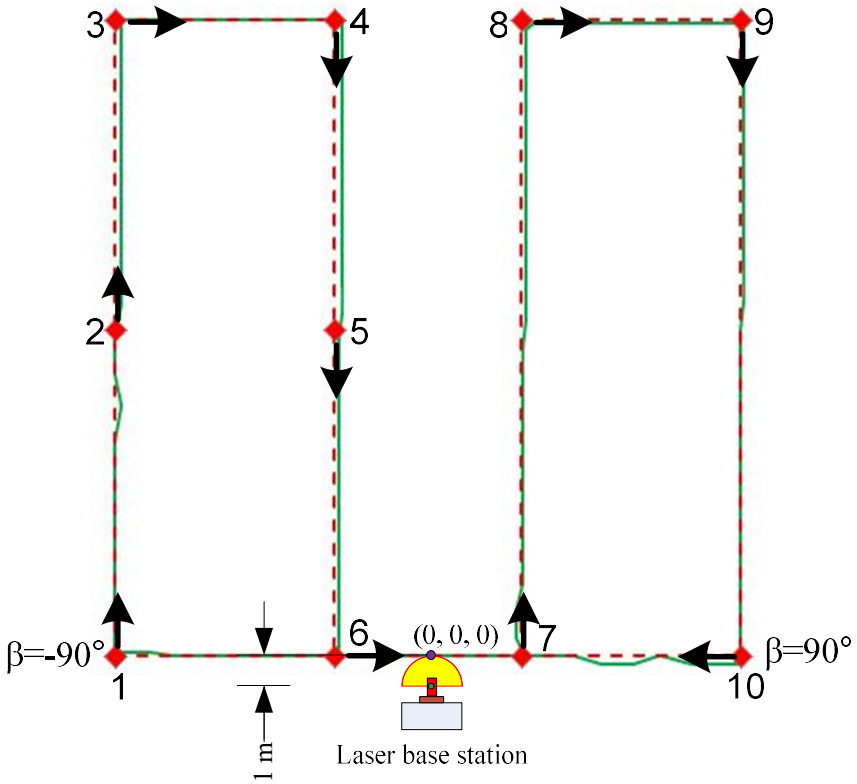

4.3 Result and Discussions

The overall localization performance and the total cost of the IMU-coupled TLG system are compared to those of the commercially available GNSS-INS systems, namely NovAtel PwrPak7D-E2 and Trimble BX992. The performance comparison criteria are lateral accuracy (A_{OA}^{LAT}) and heading accuracy (A_{OA}^{α}). The lateral accuracy of the IMU-coupled TLG system is computed from the overall XYZ accuracies (A_{OA}^{X} and A_{OA}^{Y} as shown in Table 4.4) using the equations as follows:

$$A_{OA}^{LAT} = \sqrt{(A_{OA}^{X})^2 + (A_{OA}^{Y})^2} \tag{13}$$

The comparison of the IMU-coupled TLG system with the NovAtel PwrPak7D-E2 and Trimble BX992 is summarized in Table 4.5. The lateral and heading accuracies of NovAtel PwrPak7D-E2 and Trimble BX992 are based on the best performance claimed by their system specifications. The lateral accuracies of the IMU-coupled TLG system (on flat field), NovAtel PwrPak7D-E2, and Trimble BX992 are 1.68 cm, 1.00 cm, 5.00 cm, respectively. The heading accuracies of the IMU-coupled TLG system (on flat field), NovAtel PwrPak7D-E2, and Trimble BX992 are 0.90º, 0.05º, and 0.09º, respectively. This shows that the localization performance of the IMU-coupled TLG system is comparable to those of the commercially available GNSS-INS systems. Furthermore, while the GNSS-INS systems are limited only for an open, outdoor environment under optimal open-sky conditions, the IMU-coupled TLG system can operate in both indoor and outdoor settings with the only outdoor limitations of rainy weather and maximum light intensity of 20,000 lux (at PMT).

Table 4.5

Comparison of Lateral/Heading Accuracy and Total Cost of the IMU-Coupled TLG System to the Commercially Available GNSS-INS Systems, NovAtel PwrPak7D-E2 and Trimble BX992

Overall Accuracy	IMU-coupled TLG	NovAtel PwrPak7D-E2	Trimble BX992
Lateral (A_{OA}^{LAT})	1.68 cm	1.00 cm	5.00 cm
Heading (A_{OA}^{a})	0.90º	0.05º	0.09º
Total Cost (USD)	~$950	~$11,000	~$6,000

4.4 Chapter Summary

The total cost of the IMU-coupled TLG system is approximately $950 in USD, while those of NovAtel PwrPak7D-E2 and Trimble BX992 are approximately $11,000 in USD and $6,000 in USD, respectively. The costs of the NovAtel PwrPak7D-E2 and Trimble BX992 are based on the actual online prices in February 2021, which may vary depending on the location. Also, there is an additional yearly cost for GNSS correction services, i.e., for this instance, TerraStar for NovAtel GNSS receivers and Trimble-RTX for Trimble receivers. The prices and availability of the GNSS correction services may vary depending on the geographical location. If the GNSS correction service is unavailable in the desired area of operation, a separate GNSS base is required, which may add up to $12,000 in USD into the total cost of the GNSS-INS system. This can be concluded that the total cost of the IMU-coupled TLG system is at least five times less expensive compared to the commercially available GNSS-INS systems in the current market. The IMU-coupled TLG system comes with enough position and orientation accuracy for agriculture factories.

CHAPTER 5
CONCLUSIONS AND RECOMMENDATIONS

5.1 Summary and Conclusion

The experimental results of the flat field and the paddy field showed similar localization performance; only the highest position error between points 10 and 7 in Figure 4.5 comes from an uneven surface on the paddy field. The repeated robot's position and orientation measurements on a 20 x 21 m flat, open area, the IMU-coupled TLG system with a total cost of only $950 in USD can achieve the lateral and heading accuracy of 1.68 cm and 0.90º in the flat field and 1.72 cm and 1.0º in the paddy field, respectively. The lateral and heading accuracy performances are comparable to those of commercially available GNSS-INS localization systems (updated in 2021). The multipass horizontal path tracking also confirmed the high accuracy and precision of the IMU-coupled TLG system. Furthermore, the IMU-coupled TLG system reliably performed various light intensities on the laser targets under 20,000 lux without any noticeable deterioration in localization accuracy and precision. Hence, this novel IMU-coupled TLG system presents a new promising solution as a low-cost, high-accuracy alternative for automatic machinery in farms and agricultural industries.

5.2 Recommendation for Future Research

To apply the localization system in a paddy field for commercial or self-farm use, some improvements want to modify as follow:

- Replace the camera sensor behind the laser target with an RGB light sensor array to reduce the target size and improve sensor sensibility and accuracy.
- Add an auto-leveling system for the laser base unit. The added auto-leveling unit helps the system find the ground plane quickly.
- Make a trailer to carry the system anywhere.
- Redesign the case cover to protect moisture.
- Adding a solar cell system to supply most equipment.
- Mark the reference points to the paddy fields for easy installation and convert relative position to absolute position.

REFERENCES

Aghili, F., and Salerno, A. (2009). Attitude determination and localization of mobile robots using two RTK GPSs and IMU. 2009 IEEE/RSJ International Conference on Intelligent Robots and Systems, IROS 2009, 2045–2052. https://doi.org/10.1109/IROS.2009.5354770

Backman, J., Oksanen, T., and Visala, A. (2012). Navigation system for agricultural machines: Nonlinear Model Predictive path tracking. Computers and Electronics in Agriculture, 82, 32–43. https://doi.org/10.1016/j.compag.2011.12.009

Bento, L. C., Nunes, U., Moita, F., and Surrecio, A. (2005). Sensor fusion for precise autonomous vehicle navigation in outdoor semi-structured environments. IEEE Conference on Intelligent Transportation Systems, Proceedings, ITSC, 2005(3), 245–250. https://doi.org/10.1109/ITSC.2005.1520055

Betke, M., and Gurvits, L. (1997). Mobile robot localization using landmarks. IEEE Transactions on Robotics and Automation, 13(2), 251–263. https://doi.org/10.1109/70.563647

Borenstein, J., Everett, H. R., Feng, L., and Wehe, D. (1997). Mobile robot positioning: Sensors and techniques. Journal of Robotic Systems, 14(4), 231–249. https://doi.org/10.1002/(SICI)1097-4563(199704)14:4<231::AID-ROB2>3.0.CO;2-R

Canedo-Rodríguez, A., Álvarez-Santos, V., Regueiro, C. V., Iglesias, R., Barro, S., and Presedo, J. (2016). Particle filter robot localisation through robust fusion of laser, WiFi, compass, and a network of external cameras. Information Fusion, 27, 170–188. https://doi.org/10.1016/j.inffus.2015.03.006

Corbellini, S., Ferraris, F., and Parvis, M. (2006). Low-cost laser-based localization system for agricultural machines. IEEE Transactions on Instrumentation and Measurement, 55(5), 1530–1535. https://doi.org/10.1109/imtc.2005.1604256

Dai, K., Wang, Y., Hu, J. S., Nam, K., and Yin, C. (2020). Intertarget Occlusion Handling in Multiextended Target Tracking Based on Labeled Multi-Bernoulli Filter Using Laser Range Finder. IEEE/ASME Transactions on Mechatronics, 25(4), 1719–1728. https://doi.org/10.1109/TMECH.2020.2994066

De-La-Llana-calvo, Á., Salido-Monzú, D., Lázaro-Galilea, J. L., Gardel-Vicente, A., Bravo-Muñoz, I., and Rubiano-Muriel, B. (2020). Accuracy and precision

assessment of AOA-based indoor positioning systems using infrastructure lighting and a position-sensitive detector. Sensors (Switzerland), 20(18), 5359. https://doi.org/10.3390/s20185359

Emter, T., Saltoğlu, A., and Petereit, J. (2010). Multi-sensor fusion for localization of a mobile robot in outdoor environments. Joint 41st International Symposium on Robotics and 6th German Conference on Robotics 2010, ISR/ROBOTIK 2010, 1–6.

Emter, T., and Ulrich, T. (2012). Fusion of geometrical and visual information for localization and mapping in outdoor environments. 2012 Ubiquitous Positioning, Indoor Navigation, and Location Based Service, UPINLBS 2012, 1–5. https://doi.org/10.1109/UPINLBS.2012.6409748

English, A., Ball, D., Ross, P., Upcroft, B., Wyeth, G., and Corke, P. (2013). Low cost localisation for agricultural robotics. Proceedings of the 2013 Australasian Conference on Robotics and Automation, 1–8.

Fang, H., Yang, M., Yang, R., and Wang, C. (2009). Ground-Texture-Based Localization for Intelligent Vehicles. IEEE Transactions on Intelligent Transportation Systems, 10(3), 463–468. https://doi.org/10.1016/s0965-206x(98)80022-3

Gan-Mor, S., Clark, R. L., and Upchurch, B. L. (2007). Implement lateral position accuracy under RTK-GPS tractor guidance. Computers and Electronics in Agriculture, 59(1–2), 31–38. https://doi.org/10.1016/j.compag.2007.04.008

Gao, J., Petovello, M. G., and Cannon, M. E. (2007). GPS/low-cost IMU/onboard vehicle sensors integrated land vehicle positioning system. Eurasip Journal on Embedded Systems, 2007, 1–14. https://doi.org/10.1155/2007/62616

Gomez-Gil, J., Alonso-Garcia, S., Gómez-Gil, F. J., and Stombaugh, T. (2011). A simple method to improve autonomous GPS positioning for tractors. Sensors, 11(6), 5630–5644. https://doi.org/10.3390/s110605630

Guan, R. P., Ristic, B., Wang, L., and Evans, R. (2018). Monte Carlo localisation of a mobile robot using a Doppler–Azimuth radar. Automatica, 97, 161–166. https://doi.org/10.1016/j.automatica.2018.08.012

Gui, P., Tang, L., and Mukhopadhyay, S. (2015). MEMS based IMU for tilting measurement: Comparison of complementary and kalman filter based data fusion. Proceedings of the 2015 10th IEEE Conference on Industrial

Electronics and Applications, ICIEA 2015, 2004–2009. https://doi.org/10.1109/ICIEA.2015.7334442

Guo, J., Li, X., Li, Z., Hu, L., Yang, G., Zhao, C., Fairbairn, D., Watson, D., and Ge, M. (2018). Multi-GNSS precise point positioning for precision agriculture. Precision Agriculture, 19(5), 895–911. https://doi.org/10.1007/s11119-018-9563-8

Hague, T., Marchant, J. A., and Tillett, N. D. (2000). Ground based sensing systems for autonomous agricultural vehicles. Computers and Electronics in Agriculture, 25(1–2), 11–28. https://doi.org/10.1016/S0168-1699(99)00053-8

Han, X. Z., Kim, H. J., Kim, J. Y., Yi, S. Y., Moon, H. C., Kim, J. H., and Kim, Y. J. (2015). Path-tracking simulation and field tests for an auto-guidance tillage tractor for a paddy field. Computers and Electronics in Agriculture, 112, 161–171. https://doi.org/10.1016/j.compag.2014.12.025

He, G., Yuan, X., Zhuang, Y., and Hu, H. (2020). An Integrated GNSS/LiDAR-SLAM Pose Estimation Framework for Large-Scale Map Building in Partially GNSS-Denied Environments. IEEE Transactions on Instrumentation and Measurement, 70, 1–9. https://doi.org/10.1109/TIM.2020.3024405

Her, K. W., Kim, D. H., and Ha, J. E. (2012). Localization of mobile robot using laser range finder and IR landmark. International Conference on Control, Automation and Systems, 459–461.

Hoppenot, P., and Colle, E. (1997). Real-Time Mobile Robot Localisation with Poor Ultrasonic Data. IFAC Proceedings Volumes, 30(7), 131–136. https://doi.org/10.1016/s1474-6670(17)43252-6

Hsu, W. L., Chen, O., and Huang, S. K. (2007). Localization based on magnetic and RSS data fusion with covariance intersection for mobile sensor network. IEEE/ASME International Conference on Advanced Intelligent Mechatronics, AIM, 1–6. https://doi.org/10.1109/AIM.2007.4412561

Jilek, T. (2015). Autonomous field measurement in outdoor areas using a mobile robot with RTK GNSS. IFAC-PapersOnLine, 28(4), 480–485. https://doi.org/10.1016/j.ifacol.2015.07.081

Kato, Y., and Morioka, K. (2019). Autonomous Robot Navigation System Without Grid Maps Based on Double Deep Q-Network and RTK-GNSS Localization in Outdoor Environments. Proceedings of the 2019 IEEE/SICE International

Symposium on System Integration (SII), 346–351. https://doi.org/10.1109/SII.2019.8700426

Larsson, U., Forsberg, J., and Wernersson, A. (1996). Mobile robot localization: integrating measurements from a time-of-flight laser. IEEE Transactions on Industrial Electronics, 43(3), 422–431. https://doi.org/10.1109/41.499815

Le, T., Omholt Gjevestad, J. G., and From, P. J. (2019). Online 3D Mapping and Localization System for Agricultural Robots. IFAC-PapersOnLine, 52(30), 167–172. https://doi.org/10.1016/j.ifacol.2019.12.516

Lee, D., Son, S., Yang, K., Park, J., and Lee, H. (2009). Sensor fusion localization system for outdoor mobile robot. ICCAS-SICE 2009 - ICROS-SICE International Joint Conference 2009, Proceedings, 1384–1387.

Lenain, R., Thuilot, B., Cariou, C., and Martinet, P. (2006). High accuracy path tracking for vehicles in presence of sliding: Application to farm vehicle automatic guidance for agricultural tasks. Autonomous Robots, 21(1), 79–97. https://doi.org/10.1007/s10514-006-7806-4

LeVoir, S. J., Farley, P. A., Sun, T., and Xu, C. (2020). High-Accuracy Adaptive Low-Cost Location Sensing Subsystems for Autonomous Rover in Precision Agriculture. IEEE Open Journal of Industry Applications, 1(September), 74–94. https://doi.org/10.1109/ojia.2020.3015253

LI, B., and Teunissen, P. J. (2012). Real-Time Kinematic positioning using fused data from multiple GNSS antennas. 2012 15th International Conference on Information Fusion, 933–938. https://ieeexplore.ieee.org/document/6289902

Li, J., Zhang, L., and Yang, Q. (2020). Development of Land Leveling Equipment Based on GNSS. 2020 IEEE 5th International Conference on Signal and Image Processing, ICSIP 2020, 1056–1059. https://doi.org/10.1109/ICSIP49896.2020.9339436

Li, P., Huang, J., Wan, M., Wang, S., and Wang, Y. (2012). Basic localization alogrithm using cubature Kalman filter based on encoder and laser. International Conference on Signal Processing Proceedings, ICSP, 3, 2300–2303. https://doi.org/10.1109/ICoSP.2012.6492040

Libby, J., and Kantor, G. (2011). Deployment of a point and line feature localization system for an outdoor agriculture vehicle. Proceedings - IEEE International Conference on Robotics and Automation, 1565–1570. https://doi.org/10.1109/ICRA.2011.5980430

Mayer, P., Magno, M., Berger, A., and Benini, L. (2021). RTK-LoRa: High-Precision, Long-Range, and Energy-Efficient Localization for Mobile IoT Devices. IEEE Transactions on Instrumentation and Measurement, 70, 1–11. https://doi.org/10.1109/TIM.2020.3042296

Min, H. G., and Jeung, E. T. (2015). Complementary Filter Design for Angle Estimation using MEMS Accelerometer and Gyroscope. Departement of Control and Instrumentation, 641–773.

Mizushima, A., Ishii, K., Noguchi, N., Matsuo, Y., and Lu, R. (2011). Development of a low-cost attitude sensor for agricultural vehicles. Computers and Electronics in Agriculture, 76(2), 198–204. https://doi.org/10.1016/j.compag.2011.01.017

Moreira, A. P., Costa, P., and Lima, J. (2020). New Approach for Beacons Based Mobile Robot Localization using Kalman Filters. Procedia Manufacturing, 51, 512–519. https://doi.org/10.1016/j.promfg.2020.10.072

Nagasaka, Y., Saito, H., Tamaki, K., Seki, M., Kobayashi, K., and Taniwaki, K. (2009). An autonomous rice transplanter guided by global positioning system and inertial measurement unit. Journal of Field Robotics, 26(6–7), 537–548. https://doi.org/10.1002/rob

Nemec, D., Šimák, V., Janota, A., Hruboš, M., and Bubeníková, E. (2019). Precise localization of the mobile wheeled robot using sensor fusion of odometry, visual artificial landmarks and inertial sensors. Robotics and Autonomous Systems, 112, 168–177. https://doi.org/10.1016/j.robot.2018.11.019

Ngo, T., Nguyen, P., Huynh, S., Le, S., and Nguyen, T. (2017). Experimental comparison of Complementary filter and Kalman filter design for low-cost sensor in quadcopter. 2017 International Conference on System Science and Engineering (ICSSE), 3, 488–493.

Nilwong, S., Hossain, D., Kaneko, S. I., and Capi, G. (2019). Deep learning-based landmark detection for mobile robot outdoor localization. Machines, 7(2), 25. https://doi.org/10.3390/machines7020025

Niu, Z., Zhao, X., Sun, J., Tao, L., and Zhu, B. (2020). A Continuous Positioning Algorithm Based on RTK and VI-SLAM With Smartphones. IEEE Access, 8, 185638–185650. https://doi.org/10.1109/access.2020.3028119

Perez-Ruiz, M., Slaughter, D. C., Gliever, C., and Upadhyaya, S. K. (2012). Tractor-based Real-time Kinematic-Global Positioning System (RTK-GPS) guidance system for geospatial mapping of row crop transplant. Biosystems Engineering, 111(1), 64–71. https://doi.org/10.1016/j.biosystemseng.2011.10.009

Pini, M., Marucco, G., Falco, G., Nicola, M., and De Wilde, W. (2020). Experimental Testbed and Methodology for the Assessment of RTK GNSS Receivers Used in Precision Agriculture. IEEE Access, 8, 14690–14703. https://doi.org/10.1109/ACCESS.2020.2965741

Pititeeraphab, Y., Jusing, T., Chotikunnan, P., Thongpance, N., Lekdee, W., and Teerasoradech, A. (2016). The effect of average filter for complementary filter and Kalman filter based on measurement angle. 2016 9th Biomedical Engineering International Conference (BMEiCON), 1–4.

Reid, J. F., Zhang, Q., Noguchi, N., and Dickson, M. (2000). Agricultural automatic guidance research in North America. Computers and Electronics in Agriculture, 25(1–2), 155–167. https://doi.org/10.1016/S0168-1699(99)00061-7

Rovira-Más, F., Zhang, Q., and Reid, J. F. (2008). Stereo vision three-dimensional terrain maps for precision agriculture. Computers and Electronics in Agriculture, 60(2), 133–143. https://doi.org/10.1016/j.compag.2007.07.007

Shalal, N., Low, T., McCarthy, C., and Hancock, N. (2015a). Orchard mapping and mobile robot localisation using on-board camera and laser scanner data fusion - Part A: Tree detection. Computers and Electronics in Agriculture, 119, 254–266. https://doi.org/10.1016/j.compag.2015.09.025

Shalal, N., Low, T., McCarthy, C., and Hancock, N. (2015b). Orchard mapping and mobile robot localisation using on-board camera and laser scanner data fusion - Part B: Mapping and localisation. Computers and Electronics in Agriculture, 119, 267–278. https://doi.org/10.1016/j.compag.2015.09.026

Sheinker, A., Ginzburg, B., Salomonski, N., Frumkis, L., and Kaplan, B. Z. (2013). Localization in 2D using beacons of low frequency magnetic field. IEEE Journal of Selected Topics in Applied Earth Observations and Remote Sensing, 6(2), 1020–1030. https://doi.org/10.1109/JSTARS.2012.2213240

Shi, D., Mi, H., Collins, E. G., and Wu, J. (2020). An Indoor Low-Cost and High-Accuracy Localization Approach for AGVs. IEEE Access, 8, 50085–50090. https://doi.org/10.1109/ACCESS.2020.2980364

Shim, J. H., and Cho, Y. I. (2015). A mobile robot Localization using external surveillance cameras at indoor. Procedia Computer Science, 56(1), 502–507. https://doi.org/10.1016/j.procs.2015.07.242

Singh, R., Gehlot, A., Thakur, A. K., and Mohan, P. (2019). Outdoor localization of robot with rssi for iot connected smart devices. International Journal of Recent Technology and Engineering, 8(3), 2050–2054. https://doi.org/10.35940/ijrte.C4538.098319

Sippel, M., Kuntz, W., and Reindl, L. (2008). GNSS augmented with precise laser tracking. Record - IEEE PLANS, Position Location and Navigation Symposium, 886–891. https://doi.org/10.1109/PLANS.2008.4569996

Souvestre, F., Hafez, M., and Regnier, S. (2009). A novel laser-based tracking approach for wide field of view for robotics applications. ISOT 2009 - International Symposium on Optomechatronic Technologies, 328–333. https://doi.org/10.1109/ISOT.2009.5326043

Sun, H., Slaughter, D. C., Ruiz, M. P., Gliever, C., Upadhyaya, S. K., and Smith, R. F. (2010). RTK GPS mapping of transplanted row crops. Computers and Electronics in Agriculture, 71(1), 32–37. https://doi.org/10.1016/j.compag.2009.11.006

Tatarnikov, D., Stepanenko, A., and Astakhov, A. (2017). Backfire helix antennas for mm precision of satellite positioning in real time. Electromagnetics Research Symposium-Spring (PIERS), 479–483. https://doi.org/10.1109/PIERS.2017.8261789

Valente, D. S. M., Momin, A., Grift, T., and Hansen, A. (2020). Accuracy and precision evaluation of two low-cost RTK global navigation satellite systems. Computers and Electronics in Agriculture, 168(December 2019), 105142. https://doi.org/10.1016/j.compag.2019.105142

Wei, L., Cappelle, C., and Ruichek, Y. (2013). Camera/laser/gps fusion method for vehicle positioning under extended nis-based sensor validation. IEEE Transactions on Instrumentation and Measurement, 62(11), 3110–3122. https://doi.org/10.1109/TIM.2013.2265476

Weinstein, A. J., and Moore, K. L. (2010). Pose estimation of Ackerman steering vehicles for outdoors autonomous navigation. Proceedings of the IEEE International Conference on Industrial Technology, 579–584. https://doi.org/10.1109/ICIT.2010.5472738

Weng, Y., Wang, S., Zhang, H., Gu, H., and Wei, X. (2017). A high resolution tilt measurement system based on multi-accelerometers. Measurement: Journal of the International Measurement Confederation, 109(May), 215–222. https://doi.org/10.1016/j.measurement.2017.05.058

Xue, J., Zhang, L., and Grift, T. E. (2012). Variable field-of-view machine vision based row guidance of an agricultural robot. Computers and Electronics in Agriculture, 84, 85–91. https://doi.org/10.1016/j.compag.2012.02.009

YIN, X., DU, J., GENG, D., and JIN, C. (2018). Development of an automatically guided rice transplanter using RTK-GNSS and IMU. IFAC-PapersOnLine, 51(17), 374–378. https://doi.org/10.1016/j.ifacol.2018.08.193

Zekavat, R., and Buehrer, R. M. (2011). Handbook of position location: Theory, practice and advances. In Handbook of Position Location. John Wiley & Sons. https://doi.org/10.1002/9781119434610

Zhang, Q., and Pierce, F. J. (2013). Agricultural automation: Fundamentals and practices. crc Press.

Zhang, R. G., Shen, F., and Li, Q. H. (2020). A Hybrid Indoor/Outdoor Positioning and Orientation Solution Based on INS, UWB and Dual-Antenna RTK-GNSS. 27th Saint Petersburg International Conference on Integrated Navigation Systems, ICINS 2020 - Proceedings, 1–5. https://doi.org/10.23919/ICINS43215.2020.9133911

Zhang, R., Shen, F., and Li, Q. H. (2020, May 1). A Hybrid Indoor/Outdoor Positioning and Orientation Solution Based on INS, UWB and Dual-Antenna RTK-GNSS. 27th Saint Petersburg International Conference on Integrated Navigation Systems, ICINS 2020 - Proceedings. https://doi.org/10.23919/ICINS43215.2020.9133911

Zhe, Z., Wang, J. Bin, Bo, S., and Tong, G. F. (2020). Adaptive Complementary Filtering Algorithm for IMU Based on MEMS. Proceedings of the 32nd Chinese Control and Decision Conference, CCDC 2020, 5409–5416. https://doi.org/10.1109/CCDC49329.2020.9164809

Zhu, Z., Chiu, H. P., Oskiper, T., Ali, S., Hadsell, R., Samarasekera, S., and Kumar, R. (2011). High-precision localization using visual landmarks fused with range data. Proceedings of the IEEE Computer Society Conference on Computer Vision and Pattern Recognition (CVPR), 81–88. https://doi.org/10.1109/CVPR.2011.5995463

VITA

Supod Kaewkorn received his B.Eng. degree in electrical engineering from Kasembundit University, Bangkok, Thailand in 1998, his M.Eng. degree in computer engineering from King Mongkut's University of Technology Ladkrabang, Bangkok, Thailand in 2003. He joined the Mechatronics Engineering Technology Division, Department of Mechanical Engineering Technology, College of Industrial Technology, King Mongkut's University of Technology North Bangkok in 2010, where he currently is an Assistant Professor. Also, he is a Ph.D. student in mechatronics at the School of Engineering and Technology, Asian Institute of Technology, Pathumthani, Thailand. His research interests include automatic control systems, computer control, microcontroller, deep learning, and Embedded Systems.